Research on Chemical Intermediates (2023) 49:2455–2493
https://doi.org/10.1007/s11164-023-04991-y

Synthesis, structure elucidation, antioxidant, antimicrobial, anti-inflammatory and molecular docking studies of transition metal(II) complexes derived from heterocyclic Schiff base ligands

Binesh Kumar[1] · Jai Devi[1] · Anju Manuja[2]

Received: 3 January 2023 / Accepted: 25 February 2023 / Published online: 10 March 2023

Abstract

In the search of significant biological agents for the pathogenic causing deformities, four bidentate heterocyclic Schiff base ligands and their sixteen Co(II), Ni(II), Cu(II) and Zn(II) metal complexes were derived by the condensation of 3,4-dihydro-2H-1,5-benzodioxepin-7-amine with salicylaldehyde derivatives/2-hydroxy-1-naphthaldehyde. Further, the synthesized compounds were characterized by numerous analytical techniques such as NMR, FT-IR, UV–Vis, SEM, EDAX, mass spectrometry, ESR, powder XRD, TGA, magnetic susceptibility, elemental analysis, magnetic susceptibility and molar conductance measurement for structural elucidation. The antioxidant ability of the compounds was examined by DPPH and ABTS assays while the antimicrobial (against *Staphylococcus aureus*, *Bacillus subtilis*, *Escherichia coli*, *Pseudomonas aeruginosa*, *Rhizopus oryzae* and *Candida albicans* microbial strains) and anti-inflammatory activities of the synthesized compounds were evaluated by serial dilution and egg albumin assays, respectively. The results of pharmacological activities showed that the ligand $\mathbf{HL^4}$ **(4)** and Cu(II) complexes have significant antioxidant activity while the ligand $\mathbf{HL^2}$ **(2)** and Zn(II) complexes have excellent antimicrobial and anti-inflammatory activities because of their dependency on electron donating and electron withdrawing groups, respectively. Further, the cytotoxic study was carried out for the most potent antimicrobial and anti-inflammatory $\mathbf{HL^2}$ **(2)**, $\mathbf{HL^3}$ **(3)** ligands and their **(9–16)** metal complexes on Vero cell lines using calorimetric assay which revealed that the complex **(12)** is lesser cytotoxic than the other tested compounds. After that, the less cytotoxic and more potential antimicrobial Zn(II) complex **(12)** and its ligand $\mathbf{HL^2}$ **(2)** were assessed by molecular docking study to know the interaction modes and binding affinity of these compounds with the active sites of *Staphylococcus aureus* S1: DHFR, *Escherichia coli* DNA gyrase B and *Candida albicans* sterol-14-alpha-demethylase enzymes.

Extended author information available on the last page of the article

Keywords Heterocyclic · Transition metal · Ligand · Biological activity · Molecular docking

Introduction

The progress of medicinal chemistry begun in eighteenth century in enthusiastic environment. Many researchers attempted to synthesize and design pharmaceutical agents [1, 2] and bioactive compounds that require biological importance on living system and human body. These compounds are called 'drugs' which have a positive biological response on living organism. The main moto of the medicinal chemistry [3] is to examine the interaction of drugs with cells by focusing on biochemical reaction. Numerous compounds are used as drugs in pharmaceutical industry which have good therapeutic index and less cytotoxic; and used to cure many pathogenic ailments.

The pathogenic microorganisms are dangerous for living beings because as they cause mortality and morbidity in all around the world. Therefore, the bioactive agents such as plant extracts were used for fighting against various microbial diseases [4] until the discovery of penicillin (1928) and sulfa drugs (1930). Vitamin C or ascorbic acid is used as antioxidant drug [5] and aspirin is used on broad scale in current medicinal industries as the anti-inflammatory agent [6] to remove harmful elements and damaged tissues from the body to relieve organisms from various illness. The synthetic, natural and semi-synthetic agents with a particular mechanism are able to alter in the physiological and metabolic levels by including modification on cell walls. But the excessive use of these agents has negative impact on the functioning of the body which leads to aging, cell damages, organs failure and sometime major cause of death. Furthermore, the development of potential antipathogen is currently unmet in heath cares. Hence, there is a significant need to synthesize potential pharmaceutical agents which cure the pathogenic deformities with very minimum disadvantages. So, the synthesize of a significant drug to cure the microorganism-based diseases with minimum cytotoxicity is a main objective of the present study which is based on the coordination compounds of Schiff base ligands.

Coordination complexes are a significant class of inorganic compounds which plays an important role in medicinal chemistry because they have numerous properties like denticity, flexibility, reactivity etc. The current researches deal with the coordination compounds [7, 8] of transition metals because these are essential for many biological processes and available in electron rich constituents such as nucleic acid, proteins, enzymes and carbohydrates etc. Therefore, it is necessary to research on the metal ions-based drugs, with the aim to synthesize less toxic drugs for biological systems [9]. The research in bio-inorganic chemistry has good argument to deal with Schiff base ligands-based transition metal compounds [10]. Schiff base ligands are backbone of many fields like analytical, biological, organic and inorganic industries because they have numerous features such as chelation, chemical sensors, structure modifications, reactivity etc. The activity of the ligands improved on complexation with transition metal ions due to the behavior of groups attached in the moiety, solubility, cell permeability, enzymatic action etc. Therefore, the study

of Schiff base ligand-based transition metal complexes is point of interest in the medicinal field because in the pharmaceutical industries, the widespread applicability of bioactive compounds has gained extreme propulsion of the use of transition metal complexes through the corroborative amalgamation of organic ligands as well as inorganic metal ions which offer various prospects for acquiring the potency to target the multiple biological targets in the medicinal field.

Among the transition metal complexes, Co(II), Ni(II), Cu(II), Zn(II) metal complexes have attracted the researcher due to structural flexibility, enzyme inhibitory properties, photochromic effects, penetrating power, cheating ability, good therapeutic index etc. which alter the biological response of any drug. Further, the selection of Co(II), Ni(II), Cu(II), Zn(II) metal ions in various hydrolytic enzymatic cycles among all forms of life especially carboxypeptidase, carbonic anhydrase and alcohol dehydrogenase etc. is no doubt indispensable owning to its Lewis acidity, redox inactiveness, rapid ligand exchange capability as well as flexible coordination environment. Therefore, the Co(II), Ni(II), Cu(II), Zn(II) complexes of Schiff base ligands is broadly studied in medicinal industries which have significant biological applications such as anticancer [11, 12], antifungal [13], antioxidant [14], antibacterial [15, 16], antiviral [17, 18], antituberculosis [19], anti-inflammatory [20, 21], anti-HIV [22, 23] antimalarial [24], antiparasitic [25, 26] etc.

By analyzing the significant biological importance of transition metal(II) complexes of Schiff base ligands, the synthesize of four heterocyclic ligands were carried out by condensing 3,4-dihydro-2H-benzo[b][1,4]dioxepin-7-amine (3,4-dihydro-2H-1,5-benzodioxepin-7-amine) with salicylaldehyde derivatives/2-hydroxy-1-naphthaldehyde, further which treated with Co(II), Ni(II), Cu(II) and Zn(II) acetates to form their sixteen metal(II) complexes. The characterization of the compounds was done via numerous spectroscopic and physical techniques like NMR, FT-IR, ESR, SEM, UV–Vis, mass spectrometry, molar conductance, magnetic susceptibility measurements, powder XRD, TGA and elemental analysis (CHN). The synthesized compounds were also elucidated for their in vitro biological properties against antioxidant, antimicrobial and anti-inflammatory activities. The antioxidant activity of the compounds was performed by DPPH and ABTS assays using ascorbic acid (standard drug). The antimicrobial evaluation of the synthesized compounds was assessed against six microbial strains by serial dilution methodology. Then, anti-inflammatory ability of the compounds was examined by egg albumin assay. Further, the *in vitro* cytotoxicity was evaluated for the more potent antimicrobial and anti-inflammatory ligands **HL^2 (2)**, **HL^3 (3)** and their metal complexes on Vero cells to check their toxicity level. In the recent time, the molecular docking study is highly supporting the biological ability of the compounds, therefore, the molecular docking study was implemented to examine the binding energy and interaction modes of the highly potent microbial compounds (complex **(12)** and ligand **(2)**) with the *S. aureus* S1: DHFR (2W9S), *E. coli* DNA gyrase B (4DUH) and *C. albicans* sterol-14-alpha-demethylase (5TZ1) enzymes.

Experimental

Materials

In the current research work, all the used reagents and chemicals, i.e. 3,4-dihydro-2H-benzo[b][1,4]dioxepin-7-amine (3,4-dihydro-2H-1,5-benzodioxepin-7-amine) (99%), 5-bromosalicylaldehyde (98%), 3,5-dichlorosalicylaldehyde (99%), 3-methoxy-5-nitrosalicylaldehyde (99%), 2-hydroxy-1-naphthaldehyde (98%), cobalt(II) acetate tetrahydrate, nickel(II) acetate tetrahydrate, copper(II) acetate monohydrate and zinc(II) acetate dihydrate ($\geq$98%) were of AR grade and highly pure therefore employed as such for experimental work which were purchased from Sigma-Aldrich firm.

Instruments for physical measurements

Fourier transform infrared spectra of the compounds as KBr pellets were assessed in the range of 4000–400 cm^{-1} on Perkin Elmer BX II spectrometer. The ^{13}C and ^{1}H NMR spectral data of Zn(II) metal complexes and their ligands were observed in $CDCl_3$ and DMSO-d_6 solvent on the Avance III 400 MHz:Bruker NMR instrument using tetramethylsilane (reference). The Thermo Scientific FLASH 2000 analyzer was used to obtain the elemental analysis (CHN). The ESR spectra of copper(II) complexes were observed on JES-FA200 ESR spectrometer with X-band using 3000 gauss magnetic field and TCNE (tetracyanoethylene) as standard. Molar conductivity of the 1×10^{-3} M concentration of ligands and their respective complexes in DMF solvent was assessed at room temperature by a Systronics conductivity bridge model-306. The thermogravimetric analysis was carried out at 10 °C/min heating rate by using alumina as a standard on Perkin Elmer Diamond TG/DTA thermogravimetric analyzer in atmosphere of highly pure argon having 20 mL/min flow rate. The hot-stage Gallenkamp apparatus was used to record the melting point of the compounds in open capillaries. The mass spectrometry analysis was evaluated on SCIEX Triple TOF 5600 spectrometer using acetonitrile as a solvent. UV–Vis spectra of the compounds were recorded on UV–Vis–NIR Varian Cary 5000 spectrometer at standard temperature in THF. Powder XRD of the ligands and their metal compplexes was evaluated by Rigaku Miniflex-II with Cu-Kα (1.54 Å) radiation. The value of magnetic susceptibility of the compounds was evaluated by Guoy's method taking a vibrating sample magnetometer and $Hg[Co(SCN)_4]$ as calibrant at room temperature. SEM and EDAX were recorded on JEOL 7610F plus instrument and the images of micrographs were obtained at nitrogen atmosphere.

Protocol for preparation of Schiff base ligands (HL^1-HL^4) (1–4)

The heterocyclic ligands **(1–4)** were synthesized by dissolving 3,4-dihydro-2H-benzo[b][1,4]dioxepin-7-amine (3,4-dihydro-2H-1,5-benzodioxepin-7-amine) (0.825 g, 5.0 mmol) and 5-bromosalicylaldehyde (1.005 g, 5.0 mmol)/3,5-dichlorosalicylaldehyde (0.955 g, 5.0 mmol)/3-methoxy-5-nitrosalicylaldehyde (0.985 g,

5.0 mmol)/2-hydroxy-1-naphthaldehyde (0.860 g, 5.0 mmol) in 30 mL methanol which refluxed for 5–6 h by adding 0.1 mL of glacial acetic acid. TLC was used to check the completion of reaction. After cooling, the colored precipitates were obtained at ambient temperature which were filtered, washed with hexane and finally recrystallized by methanol to purify the compounds.

Protocol for preparation of transition metal(II) complexes $[M(L^{1-4})_2(H_2O)_2]$ (5–20)

The metal(II) complexes were prepared by dissolving Co(II) acetate tetrahydrate (0.249 g), Ni(II) acetate tetrahydrate (0.248 g), Cu(II) acetate monohydrate (0.199 g), Zn(II) acetate dihydrate (0.219 g) as 1 mmol in 1:2 molar ratio with above synthesized heterocyclic ligands HL^1 (0.696 g)/HL^2 (0.676 g)/HL^3 (0.688 g)/HL^4 (0.638 g) as 2 mmol in 30 mL methanol which stirred for 3–4 h at room temperature to obtain the distinct colored precipitates that filtered and purify by washing with methanol and dried by hexane.

1. 4-bromo-2-(((3,4-dihydro-2H-benzo[b][1,4]dioxepin-7-yl)imino)methyl)phenol (HL^1)

Yield: 83%; Color: dark yellow; M.p.: 110–112 °C. Conductivity (ohm^{-1} cm^2 mol^{-1}) in DMF: 12. Anal. Calcd. (%): C, 55.19; H, 4.05; N, 4.02. Found (%): C, 55.14; H, 4.07; N, 4.05. IR (KBr, cm^{-1}): 3436 υ(O–$H_{Phenolic}$), 1057 υ(–O–CH_2–), 1621 υ(HC=N), 1309 υ(C–$O_{Phenolic}$). ^{1}H NMR (400 MHz, $CDCl_3$) δ 13.30 (s, 1H, –OH), 8.52 (s, 1H, –HC=N-), 7.50 (d, J=2.4 Hz, 1H, Ar–H), 7.46 (d, J=2.4 Hz, 1H, Ar–H), 7.04–7.02 (d, J=7.6 Hz, 1H, Ar–H), 6.97 (d, J=2.4 Hz, 1H, Ar–H), 6.94 (s, 1H, Ar–H), 6.93 (s, 1H, Ar–H), 4.30–4.26 (m, 4H, –OCH_2-), 2.28–2.22 (m, 2H, –CH_2-). ^{13}C NMR (100 MHz, $CDCl_3$) δ 160.07 (-HC=N-), 159.90 (-C–OH), 151.68, 150.70, 143.12, 135.45, 134.06, 122.19, 120.65, 119.20, 116.40, 114.06, 110.45 (Ar–C), 70.60 (-CH_2O-), 31.64 (-CH_2-). MS for $C_{16}H_{14}BrNO_3$ *m/z*: 347.0157, $[M+H]^+$: 348.0235.

2. 2,4-dichloro-6-(((3,4-dihydro-2H-benzo[b][1,4]dioxepin-7-yl)imino)methyl)phenol (HL^2)

Yield: 84%; Color: red; M.p.: 105–108 °C. Conductivity (ohm^{-1} cm^2 mol^{-1}) in DMF: 14. Anal. Calcd. (%): C, 56.82; H, 3.87; N, 4.14, Found (%): C, 56.80; H, 3.90; N, 4.18. IR (KBr, cm^{-1}): 3435 υ(O–$H_{Phenolic}$), 1042 υ(–O–CH_2–), 1610 υ(HC=N), 1304 υ(C–$O_{Phenolic}$). ^{1}H NMR (400 MHz, $CDCl_3$) δ 14.33 (s, 1H, –OH), 8.52 (s, 1H, –HC=N-), 7.46–7.45 (d, J=2.5 Hz, 1H, Ar–H), 7.02 (s, 2H, Ar–H), 6.99–6.98 (d, J=2.5 Hz, 1H, Ar–H), 6.94 (s, 1H, Ar–H), 4.30–4.26 (m, 4H, –OCH_2-), 2.28–2.22 (m, 2H, –OCH_2-). ^{13}C NMR (100 MHz, $CDCl_3$) δ 158.94 (-HC=N-), 155.94 (-C–OH), 151.72, 151.11, 141.95, 132.45, 129.56, 123.29, 122.78, 122.32, 120.28, 116.53, 114.04 (Ar–C), 70.60 (-OCH_2-), 70.58 (-OCH_2-), 31.54 (-CH_2-). MS for $C_{16}H_{13}Cl_2NO_3$ *m/z*: 337.0272, $[M+H]^+$: 338.0351.

3. 2-(((3,4-dihydro-2H-benzo[b][1,4]dioxepin-7-yl)imino) methyl)-6-methoxy-4-nitrophenol (HL^3)

Yield: 86%; Color: red; M.p.: 117–120 °C. Conductivity (ohm^{-1} cm^2 mol^{-1}) in DMF: 11. Anal. Calcd. (%): C, 59.30; H, 4.68; N, 8.14, Found (%): C, 59.35; H, 4.64; N, 8.17. IR (KBr, cm^{-1}): 3435 υ(O–$H_{Phenolic}$), 1051 υ(–O–CH_2–), 1617 υ(HC=N), 1304 υ(C–$O_{Phenolic}$). ^{1}H NMR (400 MHz, $CDCl_3$) δ 15.31 (s, 1H, –OH), 8.63 (s, 1H, –HC=N-), 8.07–8.06 (d, J=2.5 Hz, 1H, Ar–H), 7.79–7.78 (d, J=2.9 Hz, 1H, Ar–H), 7.07 (s, 1H, Ar–H), 7.05 (s, 1H, Ar–H), 7.03 (s, 1H, Ar–H), 4.32–4.28 (m, 4H, –OCH_2-), 4.03 (s, 3H, –OCH_3), 2.29–2.23 (m, 2H, –CH_2-). ^{13}C NMR (100 MHz, $CDCl_3$) δ 160.17 (-HC=N-), 158.99 (-C–OH), 151.83, 151.32, 149.46, 140.09, 138.89 122.49, 120.55, 116.30, 116.09, 113.93, 108.09 (Ar–C), 70.62 (-OCH_2-), 70.58 (-OCH_2-), 56.49 (-OCH_3), 31.44 (-CH_2-). MS for $C_{17}H_{16}N_2O_6$ *m/z:* 344.1008, $[M+H]^+$: 345.1087.

4. 1-(((3,4-dihydro-2H-benzo[b][1,4]dioxepin-7-yl)imino)methyl)naphthalen-2-ol (HL^4)

Yield: 81%; Color: brown; M.p.: 112–115 °C. Conductivity (ohm^{-1} cm^2 mol^{-1}) in DMF: 13. Anal. Calcd. (%): C, 75.12; H, 5.37; N, 4.39, Found (%): C, 75.17; H, 5.33; N, 4.43. IR (KBr, cm^{-1}): 3437 υ(O–$H_{Phenolic}$), 1062 υ(–O–CH_2–), 1620 υ(HC=N), 1311 υ(C–$O_{Phenolic}$). ^{1}H NMR (400 MHz, $CDCl_3$) δ 15.51 (s, 1H, –OH), 9.30 (s, 1H, –HC=N-), 8.11–8.09 (d, J=7.4 Hz, 1H, Ar–H), 7.82–7.79 (d, J=7.1 Hz, 1H, Ar–H), 7.74–7.72 (d, J=8.0 Hz, 1H, Ar–H), 7.55–7.51 (dd, J=7.4, 2.2 Hz, 1H, Ar–H), 7.37–7.35 (d, J=7.5 Hz, 1H, Ar–H), 7.12–7.10 (d, J=7.2 Hz, 2H, Ar–H), 7.06 (s, 1H, Ar–H), 6.99–6.97 (dd, J=7.6, 2.5 Hz, 1H, Ar–H), 4.32–4.26 (m, 4H, –OCH_2-), 2.29–2.23 (m, 2H, –CH_2-). ^{13}C NMR (100 MHz, $CDCl_3$) δ 169.48 (-HC=N-), 154.38 (-C–OH), 151.92, 150.02, 140.94, 136.33, 133.20, 129.36, 128.02, 127.33, 123.47, 122.44, 122.03, 118.90, 115.63, 113.12, 108.82 (Ar–C), 70.69 (-OCH_2-), 31.73 (-CH_2-). MS for $C_{20}H_{17}NO_3$ *m/z*: 319.1208, $[M+H]^+$: 320.1287.

5. $[Co(L^1)_2(H_2O)_2]$

Yield: 73%; Color: reddish brown; M.P.: 251–255 °C. Conductivity (ohm^{-1} cm^2 mol^{-1}) in DMF: 14. Anal. Calcd. (%): C, 48.69; H, 3.83; N, 3.55; Co, 7.47. Found (%): C, 48.65; H, 3.87; N, 3.58; Co, 7.49. IR (KBr, cm^{-1}): 3437 υ(-OH_{Water}), 1049 υ(–O–CH_2–), 1615 υ(HC=N), 1259 υ(C–$O_{Phenolic}$), 564 υ(M–O), 449 υ(M–N). MS for $C_{32}H_{30}Br_2N_2O_8Co$ *m/z*: 788.9680, $[M+H]^+$: 789.9759.

6. $[Ni(L^1)_2(H_2O)_2]$

Yield: 79%; Color: green; M.P.: 223–225 °C. Conductivity (ohm^{-1} cm^2 mol^{-1}) in DMF: 17. Anal. Calcd. (%): C, 48.71; H, 3.83; N, 3.55; Ni, 7.44. Found (%):

C, 48.68; H, 3.85; N, 3.59; Ni, 7.45. IR (KBr, cm^{-1}): 3435 υ(-OH_{Water}), 1045 υ(–O–CH_2–), 1615 υ(HC=N), 1254 υ(C–$O_{Phenolic}$), 565 υ(M–O), 495 υ(M–N). MS for $C_{32}H_{30}Br_2N_2O_8Ni$ *m/z*: 787.9702, $[M+H]^+$: 788.9780.

7. $[Cu(L^1)_2(H_2O)_2]$

Yield: 71%; Color: reddish brown; M.P.: 245–248 °C. Conductivity (ohm^{-1} cm^2 mol^{-1}) in DMF: 15. Anal. Calcd. (%): C, 48.41; H, 3.81; N, 3.53; Cu, 8.00. Found (%): C, 48.45; H, 3.77; N, 3.56; Cu, 7.99. IR (KBr, cm^{-1}): 3436 υ(-OH_{Water}), 1048 υ(–O–CH_2–), 1616 υ(HC=N), 1254 υ(C–$O_{Phenolic}$), 533 υ(M–O), 466 υ(M–N). MS for $C_{32}H_{30}Br_2N_2O_8Cu$ *m/z*: 792.9644, $[M+H]^+$: 793.9723.

8. $[Zn(L^1)_2(H_2O)_2]$

Yield: 74%; Color: light yellow; M.P.: 238–240 °C. Conductivity (ohm^{-1} cm^2 mol^{-1}) in DMF: 19. Anal. Calcd. (%): C, 48.30; H, 3.80; N, 3.52; Zn, 8.22. Found (%): C, 48.35; H, 3.75; N, 3.57; Zn, 8.20. IR (KBr, cm^{-1}): 3435 υ(-OH_{Water}), 1047 υ(–O–CH_2–), 1601 υ(HC=N), 1259 υ(C–$O_{phenolic}$), 555 υ(M–O), 449 υ(M–N). ^{1}H NMR (400 MHz, DMSO- d_6) δ 9.32 (s, 1H, –HC=N-), 8.62 (s, 1H, Ar–H), 7.11 (d, J=2.3 Hz, 2H, Ar–H), 7.09 (d, J=2.2 Hz, 2H, Ar–H), 6.90 (s, 1H, Ar–H), 3.72–3.67 (m, 4H, –OCH_2-), 2.59–2.54 (m, 2H, –CH_2-). ^{13}C NMR (100 MHz, DMSO- d_6) δ 168.68 (-HC=N-), 161.45 (-C-O-), 151.74, 151.67, 150.40, 147.73, 143.48, 128.24, 123.78, 122.13, 118.45, 116.35, 113.93 (Ar–C), 70.59 (-OCH_2-), 64.70 (-OCH_2-), 31.71 (-CH_2-). MS for $C_{32}H_{30}Br_2N_2O_8Zn$ *m/z*: 793.9640, $[M+H]^+$: 794.9718.

9. $[Co(L^2)_2(H_2O)_2]$

Yield: 72%; Color: red; M.P.: 272–275 °C. Conductivity (ohm^{-1} cm^2 mol^{-1}) in DMF: 18. Anal. Calcd. (%): C, 49.96; H, 3.67; N, 3.64; Co, 7.66. Found (%): C, 49.94; H, 3.62; N, 3.65; Co, 7.68. IR (KBr, cm^{-1}): 3437 υ(-OH_{Water}), 1035 υ(–O–CH_2–), 1595 υ(HC=N), 1266 υ(C–$O_{Phenolic}$), 537 υ(M–O), 453 υ(M–N). MS for $C_{32}H_{28}Cl_4N_2O_8Co$ *m/z*: 768.9902, $[M+H]^+$: 769.9981.

10. $[Ni(L^2)_2(H_2O)_2]$

Yield: 81%; Color: green; M.P.: 277–280 °C. Conductivity (ohm^{-1} cm^2 mol^{-1}) in DMF: 16. Anal. Calcd. (%): C, 49.97; H, 3.67; N, 3.64; Ni, 7.63. Found (%): C, 49.99; H, 3.70; N, 3.69; Ni, 7.62. IR (KBr, cm^{-1}): 3434 υ(-OH_{Water}), 1029 υ(–O–CH_2–), 1602 υ(HC=N), 1274 υ(C–$O_{Phenolic}$), 551 υ(M–O), 448 υ(M–N). MS for $C_{32}H_{28}Cl_4N_2O_8Ni$ *m/z*: 767.9924, $[M+H]^+$: 769.0002.

11. $[Cu(L^2)_2(H_2O)_2]$

Yield: 75%; Color: green; M.P.: 265–267 °C. Conductivity (ohm^{-1} cm^2 mol^{-1}) in DMF: 15. Anal. Calcd. (%): C, 49.66; H, 3.65; N, 3.62; Cu, 8.21. Found (%):

C, 49.63; H, 3.68; N, 3.67; Cu, 8.22. IR (KBr, cm^{-1}): 3432 υ(-OH_{Water}), 1057 υ(–O–CH_2–), 1595 υ(HC=N), 1296 υ(C–$O_{Phenolic}$), 539 υ(M–O), 459 υ(M–N). MS for $C_{32}H_{28}Cl_4N_2O_8Cu$ *m/z*: 772.9866, $[M+H]^+$: 773.9945.

12. $[Zn(L^2)_2(H_2O)_2]$

Yield: 76%; Color: light yellow; M.P.: 258–260 °C. Conductivity (ohm^{-1} cm^2 mol^{-1}) in DMF: 16. Anal. Calcd. (%): C, 49.54; H, 3.64; N, 3.61; Zn, 8.43. Found (%): C, 49.57; H, 3.69; N, 3.65; Zn, 8.41. IR (KBr, cm^{-1}): 3431 υ(-OH_{Water}), 1033 υ(–O–CH_2–), 1591 υ(HC=N), 1282 υ(C–$O_{Phenolic}$), 544 υ(M–O), 463 υ(M–N). ^{1}H NMR (400 MHz, $CDCl_3$) δ 8.23 (s, 1H, –HC=N-), 7.54 (s, 1H, Ar–H), 7.13 (s, 1H, Ar–H), 6.84 (s, 1H, Ar–H), 6.67–6.66 (d, J=7.2 Hz, 1H, Ar–H), 6.65–6.64 (d, J=7.0 Hz, 1H, Ar–H), 4.22–4.16 (m, 4H, –OCH_2-), 2.21–2.16 (m, 2H, –CH_2-).^{13}C NMR (100 MHz, $CDCl_3$) δ 167.64 (-HC=N-), 164.06 (-C-O-), 151.77, 150.72, 143.17, 134.96, 133.37, 128.27, 122.48, 119.19, 118.51, 116.47, 114.06 (Ar–C), 70.53 (-OCH_2-), 70.49 (-OCH_2-), 31.40 (-CH_2-). MS for $C_{32}H_{28}Cl_4N_2O_8Zn$ *m/z*: 773.9862, $[M+H]^+$: 774.9940.

13. $[Co(L^3)_2(H_2O)_2]$

Yield: 73%; Color: light yellow; M.P.: 238–241 °C. Conductivity (ohm^{-1} cm^2 mol^{-1}) in DMF: 15. Anal. Calcd. (%): C, 52.25; H, 4.38; N, 7.17; Co, 7.54. Found (%): C, 52.27; H, 4.40; N, 7.20; Co, 7.57. IR (KBr, cm^{-1}): 3401 υ(-OH_{Water}), 1049 υ(–O–CH_2–), 1594 υ(HC=N), 1262 υ(C–$O_{Phenolic}$), 553 υ(M–O), 479 υ(M–N). MS for $C_{34}H_{34}N_4O_{14}Co$ *m/z*: 781.1404, $[M+H]^+$: 782.1482.

14. $[Ni(L^3)_2(H_2O)_2]$

Yield: 70%; Color: light green; M.P.: 241–245 °C. Conductivity (ohm^{-1} cm^2 mol^{-1}) in DMF: 17. Anal. Calcd. (%): C, 52.26; H, 4.39; N, 7.17; Ni, 7.51. Found (%): C, 52.24; H, 4.42; N, 7.19; Ni, 7.50. IR (KBr, cm^{-1}): 3431 υ(-OH_{Water}), 1046 υ(–O–CH_2–), 1613 υ(HC=N), 1261 υ(C–$O_{Phenolic}$), 552 υ(M–O), 452 υ(M–N). MS for $C_{34}H_{34}N_4O_{14}Ni$ *m/z*: 780.1425, $[M+H]^+$: 781.1503.

15. $[Cu(L^3)_2(H_2O)_2]$

Yield: 76%; Color: light green; M.P.: 222–225 °C. Conductivity (ohm^{-1} cm^2 mol^{-1}) in DMF: 14. Anal. Calcd. (%): C, 51.94; H, 4.36; N, 7.13; Cu, 8.08. Found (%): C, 51.97; H, 4.34; N, 7.15; Cu, 8.07. IR (KBr, cm^{-1}): 3421 υ(-OH_{Water}), 1044 υ(–O–CH_2–), 1614 υ(HC=N), 1258 υ(C–$O_{Phenolic}$), 533 υ(M–O), 472 υ(M–N). MS for $C_{34}H_{34}N_4O_{14}Cu$ *m/z*: 785.1368, $[M+H]^+$: 786.1446.

16. $[Zn(L^3)_2(H_2O)_2]$

Yield: 79%; Color: light orange; M.P.: 234–236 °C. Conductivity (ohm^{-1} cm^2 mol^{-1}) in DMF: 18. Anal. Calcd. (%): C, 51.82; H, 4.35; N, 7.11; Zn, 8.30.

Found (%): C, 51.85; H, 4.37; N, 7.14; Zn, 8.33. IR (KBr, cm^{-1}): 3417 υ(-OH_{Water}), 1051 υ(–O–CH_2–), 1600 υ(HC = N), 1278 υ(C–$O_{phenolic}$), 550 υ(M–O), 455 υ(M–N). ^{1}H NMR (400 MHz, $CDCl_3$) δ 8.38 (s, 1H, –HC = N-), 8.03–8.02 (d, J = 2.3 Hz, 1H, Ar–H), 7.74 (s, 1H, Ar–H), 6.87–6.85 (d, J = 8.6 Hz, 1H, Ar–H), 6.64 (s, 2H, Ar–H), 4.22–4.17 (m, 4H, –OCH_2-), 3.97 (s, 3H, –OCH_3), 2.24–2.18 (m, 2H, –CH_2-). ^{13}C NMR (100 MHz, $CDCl_3$) δ 168.11 (-HC = N-), 166.78 (-C-O-), 152.51, 151.85, 150.94, 142.71, 136.07, 125.64, 122.57, 116.28, 115.86, 114.08, 108.14 (Ar–C), 70.54 (-OCH_2-), 70.50 (-OCH_2-), 56.49 (-OCH_3), 31.31 (-CH_2-). MS for $C_{34}H_{34}N_4O_{14}Zn$ *m/z*: 786.1363, $[M + H]^+$: 787.1441.

17. $[Co(L^4)_2(H_2O)_2]$

Yield: 76%; Color: reddish brown; M.P.: 238–240 °C. Conductivity (ohm^{-1} cm^2 mol^{-1}) in DMF: 16. Anal. Calcd. (%): C, 65.66; H, 4.96; N, 3.83; Co, 8.05. Found (%): C, 65.69; H, 4.94; N, 3.85; Co, 8.04. IR (KBr, cm^{-1}): 3430 υ(-OH_{Water}), 1054 υ(–O–CH_2–), 1603 υ(HC = N), 1266 υ(C–$O_{Phenolic}$), 535 υ(M–O), 459 υ(M–N). MS for $C_{40}H_{36}N_2O_8Co$ *m/z*: 731.0968, $[M + H]^+$: 732.1046.

18. $[Ni(L^4)_2(H_2O)_2]$

Yield: 77%; Color: green; M.P.: 246–248 °C. Conductivity (ohm^{-1} cm^2 mol^{-1}) in DMF: 15. Anal. Calcd. (%): C, 65.68; H, 4.96; N, 3.83; Ni, 8.02. Found (%): C, 65.70; H, 4.97; N, 3.85; Ni, 8.03. IR (KBr, cm^{-1}): 3423 υ(-OH_{Water}), 1044 υ(–O–CH_2–), 1611 υ(HC = N), 1279 υ(C–$O_{Phenolic}$), 529 υ(M–O), 455 υ(M–N). MS for $C_{40}H_{36}N_2O_8Ni$ *m/z*: 730.1807, $[M + H]^+$: 731.1855.

19. $[Cu(L^4)_2(H_2O)_2]$

Yield: 73%; Color: green; M.P.: 227–230 °C. Conductivity (ohm^{-1} cm^2 mol^{-1}) in DMF: 17. Anal. Calcd. (%): C, 65.25; H, 4.93; N, 3.80; Cu, 8.63. Found (%): C, 65.28; H, 4.95; N, 3.83, Cu, 8.62. IR (KBr, cm^{-1}): 3431 υ(-OH_{Water}), 1044 υ(–O–CH_2–), 1613 υ(HC = N), 1260 υ(C–$O_{Phenolic}$), 522 υ(M–O), 472 υ(M–N). MS for $C_{40}H_{36}N_2O_8Cu$ *m/z*: 735.4915, $[M + H]^+$: 736.4993.

20. $[Zn(L^4)_2(H_2O)_2]$

Yield: 80%; Color: yellow; M.P.: 234–237 °C. Conductivity (ohm^{-1} cm^2 mol^{-1}) in DMF: 19. Anal. Calcd. (%): C, 65.09; H, 4.92; N, 3.80; Zn, 8.86. Found (%): C, 65.11; H, 4.95; N, 3.87; Zn, 8.88. IR (KBr, cm^{-1}): 3411 υ(-OH_{Water}), 1050 υ(–O–CH_2–), 1605 υ(HC = N), 1289 υ(C–$O_{Phenolic}$), 538 υ(M–O), 468 υ(M–N). ^{1}H NMR (400 MHz, $CDCl_3$) δ 9.29 (s, 1H, –HC = N-), 8.03–8.00 (d, J = 8.5 Hz, 1H, Ar–H), 7.82–7.79 (d, J = 7.2 Hz, 1H, Ar–H), 7.49 (d, J = 1.6 Hz, 1H, Ar–H), 7.30 (d, J = 2.1 Hz, 1H, Ar–H), 7.13–7.08 (m, 2H, Ar–H), 6.83 (s, 1H, Ar–H), 6.78–6.77 (d, J = 2.7 Hz, 1H, Ar–H), 6.74 (d, J = 2.8 Hz, 1H) 4.18–4.12 (m, 4H, –OCH_2-), 2.19–2.13 (m, 2H, –CH_2-). ^{13}C NMR (100 MHz, $CDCl_3$) δ 173.58 (-HC = N-), 162.65 (-C-O-), 154.44, 151.76, 145.36, 137.44, 135.54, 129.29, 127.87, 126.63,

122.32, 118.85, 116.68, 115.65, 114.09, 113.13, 109.04 (Ar–C), 70.68 (-OCH_2-), 70.52 (-OCH_2-), 31.62 (-CH_2-). MS for $C_{40}H_{36}N_2O_8Zn$ *m/z*: 736.4039, $[M+H]^+$: 737.4117.

Biophysical-experiments

To find out a significant medicinal agent for pathogen causing illness, we analyzed all the synthesized compounds **(1–20)** against antioxidant, antimicrobial and anti-inflammatory activities; and the highly potent antimicrobial and anti-inflammatory heterocyclic Schiff base ligands $\mathbf{HL^2}$ **(2)**, $\mathbf{HL^3}$ **(3)** and their complexes are also evaluated for cytotoxicity analysis on Vero cells to check their toxicity level.

Antioxidant activity

In vitro 2,2-dipheny-1-picrylhydrazyl (DPPH) and 2,2'-azino-bis (3-ethylbenzothiazoline-6-sulfonic acid (ABTS) assays were evaluated for a set of compounds **(1–20)** for observing the % radical scavenging and IC_{50} values using ascorbic acid (standard drug).

DPPH assay

Compound concentrations The synthesized compounds were prepared in DMSO for 200, 100, 50, 25, 12.5 µg/mL concentrations. The above prepared solutions (1 mL) were added with another 1 mL DPPH solution (1 mg DPPH in 20 mL DMSO) and dissolve the resulting solution into 1 mL DMSO [27]. Then obtained solutions were put in dark place for 30 min. after vigorous shaking.

Determination of radical scavenging activity

The diversion in absorbance of all the prepared solutions was assessed at 517 nm in triplicates by using DPPH solution in DMSO (reference). The % radical scavenging values of the compounds were assessed by using the below equation-

$$\%\text{radical scavenging value} = \left[\left(X_{\text{reference}} - Y_{\text{compound}}\right)/X_{\text{reference}}\right] \times 100$$

$X_{\text{reference}}$ - Absorbance of the reference; Y_{compound} - Absorbance of the compounds.

The graphs were plotted in between concentration (µg/mL) on X-axis and scavenging activity on Y-axis for calculating % radical scavenging; further their IC_{50} values were also calculated and compared with standard drug.

ABTS radical assay

The ABTS radical assay was performed in triplicates by producing the blue green ABTS radical cation by reacting 70 mM potassium persulfate with 7 mM ABTS in water which stored for 16 h at room temperature before use. Further, the ABTS solution was diluted with 80% methanol to obtain 0.700 ± 0.005 absorbance at 734 nm. Then mix the 2 mL ABTS solution in 100 µL solution of different concentrations (200, 100, 50, 25, 12.5 µg/mL) after that incubate the solution for 1 min at room

temperature and record the absorbance of the solutions at 734 nm by taking blank solution (2 mL ABTS solution in 200 µL methanol). A standard curve was acquired by using ascorbic acid reference solution at different concentrations. The radical scavenging ability of the compounds (1–20) was measured to calculate the IC_{50} values [30].

$$\%\text{radical scavenging value} = \left[X_{control} - Y_{compound}/X_{control}\right] \times 100$$

$X_{control}$ - Absorbance of the control (control did not have any compound or standard); $Y_{compound}$ - Absorbance of the compounds.

Antimicrobial activity

In vitro anti-fungal and anti-bacterial potential of the derived compounds were screened against two fungal and four bacterial strains (*Rhizopus oryzae* (MTCC 262), *Candida albicans* (MTCC 227), *Escherichia coli* (MTCC 732), *Pseudomonas aeruginosa* (MTCC 424), *Staphylococcus aureus* (MTCC 2901) and *Bacillus subtilis* (NCIM 2063)) via serial dilution methodology [28, 29]. Fluconazole and ciprofloxacin were taken as standard drugs for fungi and bacteria, respectively. DMSO used as negative control and the MIC (minimum inhibitory concentrations) values were recorded in the unit of µmol/mL.

Compounds concentrations

MIC values were calculated by two-fold serial dilution methodology using 1000 µg/mL stock solutions of the compounds which was prepared by dissolving 5 mg of the synthesized ligands and their complexes in 5 mL DMSO. For preparing 100 µg/mL stock solution, took 1 mL of 1000 µg/mL solution in a test tube and made up it up to 10 mL by DMSO.

Subculture of pathogens

The bacterial strains were sub-cultured in nutrient broth (NB) which was obtained by adding 1.3 g of NB in distilled water (100 mL). The fungal strains were sub-cultured in potato dextrose broth (PDB) which was obtained by adding 2.4 g of PDB in distilled water (100 mL). Both the mixtures were autoclaved for 30 min at 15 psi and the subcultures were incubated at 25 °C for seven days and at 37 °C for one day for fungal and bacterial strains, respectively.

Determination of minimum inhibitory concentration (MIC) values

The two-fold serial dilution assay was employed in triplicate manner to detect the antimicrobial properties of the compounds. In this assay, 1 mL of 100 µg/mL stock solution was added with 1 mL of broth in a test which was serially diluted for 50, 25, 12.50, 6.25 and 3.12 µg/mL concentration solutions. After that, bacteria and fungi were added in every test tube and incubated for a particular time for growth of the

culture. Growth of the pathogens was checked spectrophotometrically and visually; and record the minimum inhibitory concentrations of the compounds which were compared with reference drugs.

Anti-inflammatory activity

The in vitro anti-inflammatory evaluation of the compounds was observed in triplicate by using egg albumin method and taking diclofenac sodium as a standard drug. The solution of various concentrations was prepared in DMSO and evaluated their % inhibition and IC_{50} values.

Compound concentrations

The percentage inhibition of the compounds was evaluated by using 200, 100, 50, 25, 12.5 µg/mL concentration solutions which were obtained by mixing the compounds in the DMSO.

Determination of percentage inhibition

The above prepared solutions (2 mL) added in a test tube having egg albumin (0.2 mL of fresh hen's egg) and phosphate buffer saline (2.8 mL) of 6.4 pH. The resulting solutions of the compounds were incubated for 15–20 min at 37 °C in BOD and warmed at 70 °C for 5 min. On cooling, the alteration in absorbance of the solutions was observed at 660 nm on cooling using double distilled water as a reference/control [30, 31]. The % inhibition of the denatured protein was evaluated by the given formula-

$$\text{Percentage inhibition} = \left[X_{\text{compound}}/Y_{\text{control}} - 1\right] \times 100$$

X_{compound} - Absorbance of the compounds; Y_{control} - Absorbance of the control.

Further, the obtained IC_{50} values of the solutions were compared with the value of diclofenac sodium (standard drug).

Cytotoxicity on Vero cell lines

In vitro cytotoxic studies [32] of highly active antimicrobial and anti-inflammatory Schiff base ligands **HL^2 (2), HL^3 (3)** and their **(9–16)** complexes were performed on Vero cell lines by colorimetric assay using resazurin dye (7-hydroxy-3H-phenoxazin-3- one 10-oxide) and DMSO (reference). The resazurin dye is nonfluorescent and blue in color until reduction to highly fluorescent pink color resorufin.

Compound concentrations

Percentage cytotoxicity was calculated by using 1000 µg/mL stock solution (1 mg of compound in 10 µL DMSO and 900 µL media) which was utilized to prepare the solution of 250, 62.50 µg/mL concentration.

Subculture of cell lines

Vero cell lines were cultured in 100 µL of cell culture medium (EMEM supplemented with 10% fatal bovine serum, 25 mM sodium bicarbonate, 2 mM L-glutamine, 10 mM HEPES, amphotericin B 25 mg/mL, penicillin 10,000 units/mL, and streptomycin 10 mg/mL) at density of 1×10^4 cells per well, in 96-well cells culture plate.

Determination of percentage cytotoxicity

The above culture cells were treated with different concentrations (1000, 250 and 62.5 µg/mL) of compounds in triplicate which was incubated for 24 h at 37 °C in 5% CO_2 and incubated again for 24 h after treatment. After incubation, the compounds were treated with 10 µL of resazurin that was prepared in distilled water (1 mg/mL) and incubated again for under conditions as mentioned above which show the formation of pink color resorufin after 4 h incubation due to cellular metabolic activity. Then the absorbance of the compounds was recorded by spectrophotometer (ELISA plate reader, PowerWave™ XS2; Bio-tek, VT, USA) at 590 nm. Percentage cytotoxicity of the compounds was calculated after normalizing the background absorbance of media with reference to untreated cells [33].

$$\%\text{Cytotoxicity} = \left(X_{\text{untreated control}} - Y_{\text{compounds}}\right)/X_{\text{untreated control}} \times 100$$

X - Absorbance of the untreated control; Y - Absorbance of the compounds.

Computational study

In the recent time, the computational studies are highly supports the biological evaluation, therefore, the less cytotoxic and most antimicrobial active zinc(II) complex **(12)** and its ligand **(2)** were evaluated by molecular docking study**.**

Molecular docking

Molecular docking study was used to determine the mode of interaction and binding energy via ligand-enzyme interaction which support the biological activity of the compounds. The structure of highly microbial active and less cytotoxic compounds **(2)** and **(12)** were drawn by chemDraw3d pro and energy minimization was done by UCSF chimera. The crystal structures of the *S. aureus* S1: DHFR (PDB code-2W9S), *E. coli* DNA gyrase B (PDB code–4DUH) and *C. albicans* sterol-14-alpha-demethylase (PDB code–5TZ1) enzymes were retrieved from protein data bank (https://www.rcsb.org/); further the compounds and enzymes were docked by the Autodock Vina software. Swiss PDB application was used for structure optimization

of enzymes. The comparison and observations of the docking sites of compounds and targeted enzymes were done by BIOVIA discovery studio [34].

Results and discussion

Chemistry

In the present work, the synthesis of four heterocyclic ligands and their sixteen transition metal complexes were reported. The ligands **(1–4)** were acquired in significant amount by condensing the 3,4-dihydro-2H-benzo[b][1,4]dioxepin-7-amine (3,4-dihydro-2H-1,5-benzodioxepin-7-amine) with derivatives of salicylaldehyde/2-hydroxy-1-naphthaldehyde using methanol as solvent which further treated with methanolic solution of Co(II), Ni(II), Cu(II) and Zn(II) acetates in 1:2 molar ratio to obtain the metal(II) complexes. All the obtained compounds were solids, insoluble in the organic solvents except DMF, THF, $CDCl_3$, DMSO and stable at room temperature. The crystalline and non-electrolytic nature of the compounds were confirmed by powder XRD and molar conductance measurements, respectively. The single crystals of the compounds were not grown in numerous of attempts which carried out in different ratio of solvents. The octahedral geometry and binding sites in the complexes were confirmed by a number of spectroscopic and physical techniques which suggested that the ligands bonded to the metal centre in bidentate way by the oxygen and nitrogen atoms of the deprotonated phenolic and azomethine group, respectively.

Mass spectra

The mass spectral analysis in the positive ion mode was recorded in acetonitrile solvent that proposed the stoichiometry of the complexes [35, 36] and the obtained results are mentioned in Table S1 and Fig. S1–S8 of the supplementary. The heterocyclic Schiff ligands $\mathbf{HL^1}$, $\mathbf{HL^2}$, $\mathbf{HL^3}$ and $\mathbf{HL^4}$ shows significant ion peaks at *m/z* 348.0235, 338.0351, 345.1087 and 320.1287, respectively because of $[M+H]^+$ ion. The Co(II), Ni(II), Cu(II) and Zn(II) complexes of ligand **(4)** exhibited $[M+H]^+$ ion peak at 732.1046, 731.1855, 736.4993 and 737.4117, respectively which is same as their molecular mass ion values and confirmed octahedral geometry of the complexes. The mass spectral results confirm the complex formation of ligands with metal ion in the molar ratio of 2:1 as represented in Scheme 1.

Molar conductance measurements

The molar conductance of the compounds was recorded at ambient temperature using digital conductivity meter in 1×10^{-3} M DMF solution. The obtained conductance value exhibited in the region of 11–19 Ω^{-1} cm^2 mol^{-1} (Table S1 of the supplementary) which confirmed the non-electrolytic behavior of the compounds [37].

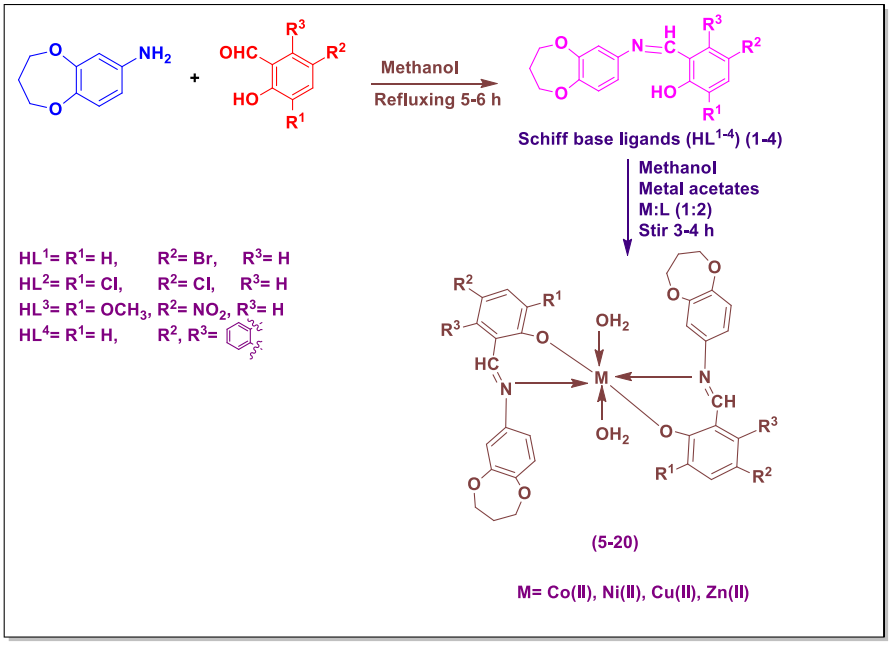

Scheme 1 Synthesis of Schiff base ligands (1–4) and their transition metal complexes (5–20)

IR spectra

The mode of coordinating sites and presence of functional groups in the compounds is examined by infrared spectroscopy at 4000 cm^{-1}–400 cm^{-1}. The obtained spectra of the ligands were compared with their respective complexes and confirmed complex formation due to appearance or disappearance of bands and shifting in frequencies because of the change in electronic environment [38, 39] (Table S2 and Fig. S9–S16 of the supplementary). In the spectra of ligands **(HL^1–HL^4)**, a strong absorption band appears near 3437–3435 cm^{-1} because of $\upsilon(O–H_{Phenolic})$ stretching vibration frequency that disappear on complexation which confirmed the bonding of ligands with metal ions. Another band appears at 1621–1610 cm^{-1} as result of $\upsilon(HC=N)$ frequency which shifts at lesser frequency after complexation shows ligation of azomethine group from N- atom to the central metal atom [40]. During complexation, there is a shifting of $\upsilon(C\text{-}O_{Phenolic})$ band frequency from 1311–1304 cm^{-1} to 1296–1254 cm^{-1} indicates bonding through deprotonated oxygen atom [41]. The IR spectra also shows a band at 1062–1029 cm^{-1} in the synthesized compounds as a result of (-O-CH_2-) group and the appearance of a broad absorption band in the complexes at 3437–3401 cm^{-1} confirmed the coordination of water molecules with central metal atom. Further, the infrared spectra of the complexes show some new bands around 565–522 cm^{-1} and 495–448 cm^{-1} which ascribed for stretching vibrations frequency of metal–oxygen (M–O) and metal-nitrogen (M–N) bonds, respectively [42]. The presence of new absorption bands in the spectra of the complexes confirms that the heteroatoms such as deprotonated oxygen atom, nitrogen atom of

–HC = N- group and oxygen atom of water molecule are bonded to the metal centre [43] which validate the octahedral nature of the complexes as shown in Scheme 1.

^{1}H NMR spectra

^{1}H NMR spectra of the heterocyclic ligands and zinc(II) complexes were carried out in DMSO- d_6 and $CDCl_3$ using trimethylsilane as a reference which are shown in Table S3 and Fig. S17–S24 of the supplementary. The **(HL^1–HL^4)** ligands shows a singlet in the region of δ 15.51–13.30 ppm due to hydroxyl proton which disappeared on complexation due to the proton abstraction of –OH group on bonding of ligands with metal centre confirm the complexation. The Schiff base ligands **(HL^1–HL^4)** have a singlet around δ 9.30–8.52 ppm because of the proton of azomethine group which was shifted at δ 9.32 ppm in case of complex **(8)** and in region of δ 9.29–8.23 ppm in the case of other complexes of zinc(II) metal, indicates chelation of azomethine nitrogen with metal. The upward shifting of peaks indicates releasing of electrons of nitrogen atom of the moiety to the zinc(II) metal centre and downward shifting of peaks might be due to the steric effects and geometry of the zinc(II) complexes [44, 45]. Some singlet, doublet and multiplet displayed around δ 8.11–6.93 ppm corresponds to the protons of phenyl ring which shifted on complexation and supports the Zn(II) complexes formation. The signal for the protons of the (-OCH_2-) groups appears near δ 4.32–4.26 ppm in ligands which gets shifted downward on complexation. A multiplet is exhibited at δ 2.29–2.22 ppm due to methylene protons, coupled with the (–OCH_2–) protons that showed shifting on complexation. Therefore, the obtained ^{1}H NMR data is supports the complex formation with ligands in 1:2 molar ratio as represented in Scheme 1.

^{13}C NMR spectra

The ^{13}C NMR spectral data of the heterocyclic ligands and Zn(II) complexes [46, 47] were observed in DMSO-d_6 and $CDCl_3$ which also supports the structures of the complexes. The obtained data displayed in Table S3 and Fig. S25–S32 of the supplementary. The **(HL^1–HL^4)** ligands shows a signal at δ 169.48–158.94 ppm because of carbon atom of of –HC = N- group which was shifted upward in the complexes, indicates bonding of nitrogen atom of the –HC = N- group to the metal centre, revealing that the electron density of N- atom of –HC = N- group shifts towards the zinc(II) metal ions. A sharp peak around δ 159.90–154.38 ppm designated for carbon atom having hydroxyl group in Schiff base ligands which was shifted around δ 166.78–161.45 ppm in the spectra of Zn(II) complexes which indicate the deprotonation of hydroxyl group by coordinating via metal ion. The signals of aromatic carbon were assigned in the region of δ 151.92–108.09 ppm for ligands and shifting of these signals clearly indicates the complexation. The **(HL^1–HL^4)** ligands shows some peaks at δ 70.69–70.58 ppm due to –OCH_2- group and at δ 31.73–31.44 ppm due to methylene group which also get shifted on complexation. The ^{13}C and ^{1}H NMR spectral data shows that the obtained signals of ligands shifted

on complexation and confirm the coordination behavior of the ligands with central metal atoms in a bidentate pattern as proposed by other techniques.

Magnetic susceptibility and electronic spectra

The UV–Vis spectral analysis of the compounds were examined in THF solvent at room temperature (Table S4 of the supplementary) which is very significant technique to confirm the stereochemistry of metal complexes. The electronic absorption spectra of ligands show strong absorption band at 25,895–27,580 cm^{-1} because of $n \rightarrow \pi^*$ transition of –HC = N- group and at 38,765–39,905 cm^{-1} as a result of $\pi \rightarrow \pi^*$ transition of aromatic ring [48, 49].

The three bands appears in Co(II) complexes in the region of 10,553–10,835 cm^{-1} for $^4T_{1g}(F) \rightarrow {}^4T_{2g}(F)$ (υ_1), 17,331–18,283 cm^{-1} for $^4T_{1g}(F) \rightarrow {}^4A_{2g}(F)$ (υ_2) and 22,583–23,154 cm^{-1} for $^4T_{1g}(F) \rightarrow {}^4T_{1g}(P)$ (υ_3) transitions that confirm octahedral environment around cobalt(II) atom which was also supported by the υ_3/υ_1, B and β values that lies at 2.11–2.19, 881.8–930.4 cm^{-1} and 0.908–0.958, respectively. The number of unpaired electron (three) in Co(II) complexes were confirmed by the magnetic moment value at 4.45–4.58 BM which also suggests octahedral behavior of cobalt(II) complexes. Ni(II) compounds also reported three absorption bands in the range of 10,251–10,982 cm^{-1} for $^3A_{2g}(F) \rightarrow {}^3T_{2g}(F)$ (υ_1), 17,018–18,867 cm^{-1} for $^3A_{2g}(F) \rightarrow {}^3T_{1g}(F)$ (υ_2) and 24,887–23,987 cm^{-1} for $^3A_{2g}(F) \rightarrow {}^3T_{1g}(P)$ (υ_3) that confirmed the octahedral behavior of the complexes. The ratio of υ_2/υ_1 nearby 1.66–1.74, the values of magnetic moment in the region of 3.35–3.52 BM, the values of ligand field parameters B nearby 683.4–743.8 cm^{-1} and β around 0.722–0.663 also support the octahedral geometry of nickel(II) complexes. The octahedral bonding around the Cu(II) metal ions was supported by 1.73–1.84 BM magnetic moment and two absorption band at 15,119–15,983 cm^{-1} for $^2B_{1g} \rightarrow {}^2A_{1g}$ (υ_1) and 23,529–24,767 cm^{-1} for $^2B_{1g} \rightarrow {}^2E_{2g}$ (υ_2) transitions. Only one absorption band shown by the Zn(II) metal complexes in the region of 22,987–23,925 cm^{-1} due to the LMCT and these complexes also have diamagnetic in nature and d^{10} configuration that confirm octahedral geometry around Zn(II) metal. The above spectral data suggests the octahedral environment for all the synthesized metal complexes as suggested by other spectral evaluations.

Powder XRD analysis

Powder XRD analysis was carried out for the synthesized compounds in the region of $2\theta = 10–80^{\circ}$ at the ambient temperature and 1.5406 Å wavelength to verify the nature of the compounds [50]. The XRD pattern of a compound is like fingerprint of the compound which analyzes amorphous and crystalline nature of the compounds, dislocation density, peak intensities and average crystallite size (D) of the compounds [51]. The crystalline nature of the compounds was confirmed by the crystalline peaks in the XRD pattern. The X-ray diffraction pattern of the ligand **(1)** and complex **(5)** are shown in Fig. 1. The Debye- Scherrer equation was used to calculate the average crystallite size (D) by the given equation

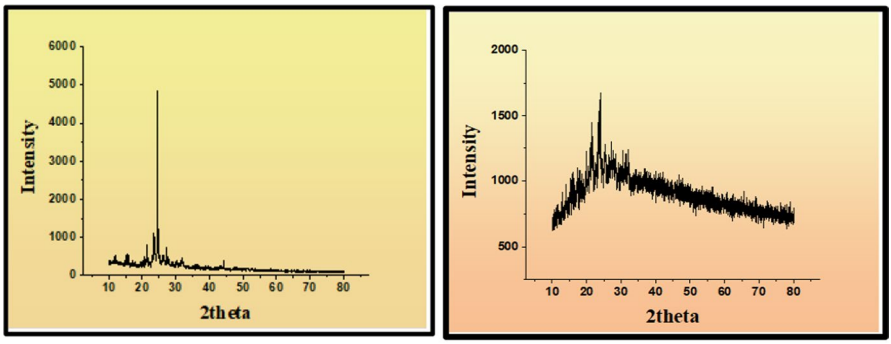

(a) (b)

Fig. 1 Powder XRD spectra **a** ligand $\mathbf{HL^1}$ (1) and **b** $[Co(L^1)_2(H_2O)_2]$ **(5)** complex

$$D_{XRD} = \frac{k\lambda}{(\beta)\cos\theta}$$

λ - wavelength (1.5406 Å); β - full width at half maximum of the reference diffraction peak; θ - diffraction angle; K - shape factor (0.95)

The ligand $\mathbf{HL^1}$ **(1)** and its Co(II) complex shows the average crystallite size (D) at 48.75 nm and 44.67 nm, respectively [52]. The complex has smaller crystallite size than its ligand due to ligation with metal ion which shows the nano-crystallite size of the complexes. The dislocation density (*δ*) of the ligand **(1)** and cobalt(II) complex **(5)** was evaluated by the below equation which is lie in the region of 0.00042–0.00050 nm^{-2} [53].

$$\delta = 1/D_{XRD}^2$$

Thermal analysis

The thermogravimetric analysis was evaluated to examine the thermal behavior of the compounds and to determine whether the H_2O molecules are outside or inside from the coordination sphere in the complexes [54–56]. The TG curve of present complexes do not indicate sharp weight loss but shows the percentage mass loss in the three steps and leaves metal oxide as residue. The results indicate the fine agreement between the proposed formulae and calculated values of the weight loss.

The thermal stabilization of the complexes was evaluated from the TG curve having function of temperature in the range of 30–900 °C. The complex $[Cu(L^1)_2(H_2O)_2]$ **(7)** do not shows any type of weight loss and stable up to 170 °C but have three decomposition steps beyond this temperature (Fig. 2). The 1st step decomposition represents the loss of the bonded water molecules from 170 to 230 °C having weight loss of 4.83% (Calcd. 4.53%). The 2nd decomposition step shows the weight loss of 46.01% (Calcd. 45.84%) around the temperature of 230–420 °C due to the loss of one ligand moiety. Further, in the 3rd step, complex decomposes in the region of

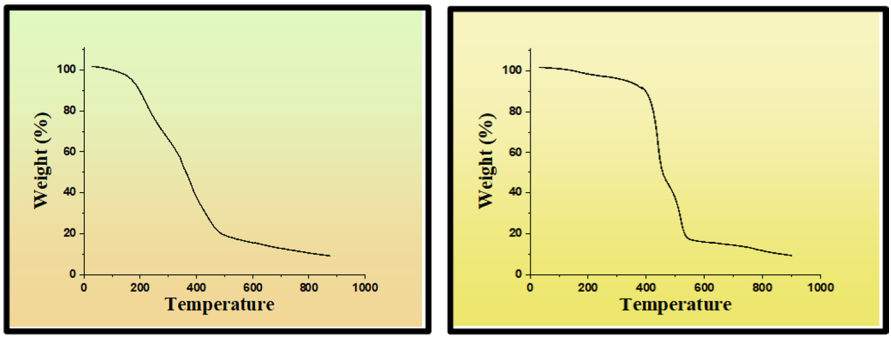

Fig. 2 TGA curves of **a** complex **(7)** **b** complex **(10)**

420–780 °C indicating weight loss of 34.57% (Calcd. 34.27%) due to another ligand moiety and leave copper oxide as the end product.

The thermal analysis curve of $[Ni(L^2)_2(H_2O)_2]$ **(10)** shows that the coordinated water molecules were loss in the first decomposition step at the temperature nearby 190–260 °C exhibiting weight loss of 4.58% (Calcd. 4.68%). Further, the complex goes for second and third steps weight loss of 46.17% (Calcd. 46.04%) and 34.71% (Calcd. 34.61%), respectively in the temperature region of 260–800 °C due to the presence of two bidentate coordinated ligands leaving behind nickel oxide as end product (Fig. 2).

The thermogravimetric evaluation of other complexes follows the same three steps for decomposition leaving metal oxide in the last which exhibit thermal stability of metal complexes up to 170 °C temperature and no weight loss was reported up to this temperature range, indicating that there is no probability of presence of H_2O molecule outer side of the coordination sphere. From thermal data, we conclude that the compounds were highly stable and non-volatile in behavior at room temperature and decomposition of synthesized compounds ends with appearance of metal oxide.

The decomposition steps of the metal compounds are as follows-

$[Cu(L^1)_2(H_2O)_2] \rightarrow [Cu(L^1)_2] + 2H_2O$	loss of two water molecules, nearby 170 – 230 °C
$[Cu(L^1)_2] \rightarrow [Cu(L^1)]$	loss of one ligand moiety, nearby 230 – 420 °C
$[Cu(L^1)] \rightarrow$ Copper oxide	loss of another ligand moiety leaving metal oxide as residue above 780 °C

SEM and EDAX analysis

SEM (scanning electron microscopy) was implemented to analyze the changes in surface morphology of Schiff base ligands on complexation [57]. The SEM micrographs of ligand $\mathbf{HL^2}$ **(2)** and its $[Co(L^2)_2(H_2O)_2]$ complex **(9)** was carried at different magnifications (Fig. 3). The micrograph of the Schiff base ligand $\mathbf{HL^2}$ **(2)** have rough surface with rectangular bars having many territorial patches and its Co(II) complex **(9)** exhibits needle shaped surface which is quite different from its Schiff base ligand. The differences in the size and shape of the particles of ligand

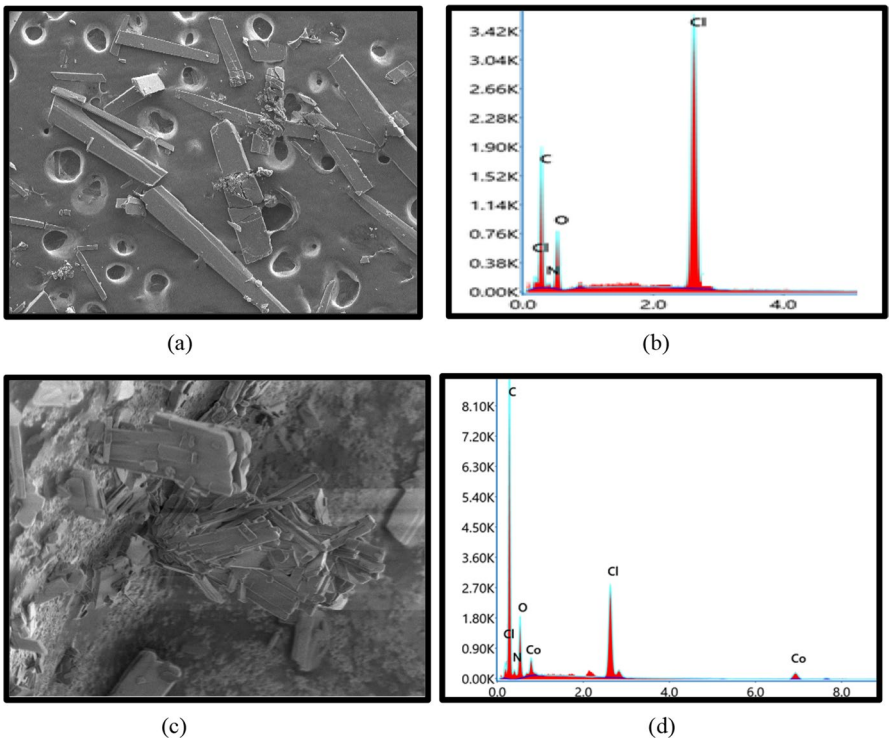

Fig. 3 **a** SEM image of HL^2 **(2)** ligand, **b** EDAX image of HL^2 **(2)** ligand, **c** SEM image of $[Co(L^2)_2(H_2O)_2]$ **(9)** complex and **d** EDAX image of $[Co(L^2)_2(H_2O)_2]$ **(9)** complex

on complexation is because of the crystal aggregation which accumulate on the thin films due to its dependency on the transition metal ions which is another evidence of complexation.

The synthesized complexes were examined by energy dispersive X-ray analysis (EDAX) to know the elemental configuration [58]. The EDAX graphs of ligand **(2)** and complex **(9)** were shown in Fig. 3. The EDAX indicates the presence of various major constitutes (C, O, N, Cl) in Schiff base ligand **(2)** and complexation was confirmed by appearance of cobalt(II) metal in the graph of complex which supports the proposed structure as shown in Scheme 1 and validate the other spectral and physical data.

Electron spin resonance spectroscopy

The ESR spectrum (solid state X-band) of copper(II) complexes were examined at liquid nitrogen temperature (77 K) and at room temperature (300 K) as shown in Fig. 4 [59, 60]. The $g_{\parallel}$ and $g_{\perp}$ values of copper(II) complexes were evaluated and reported in Table 1. The values of $g_{\parallel}$ and $g_{\perp}$ at 2.23 and 2.07 for Cu(II) complex **(15)** is according to $g_{\parallel} > g_{\perp} > 2.0023$, that supports the octahedral geometry

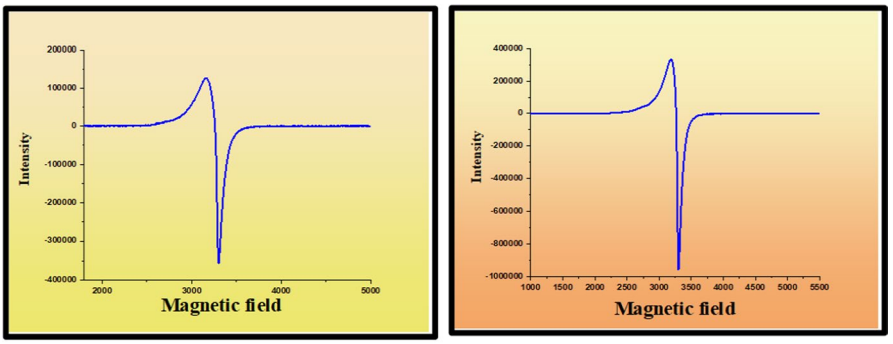

(a) (b)

Fig. 4 ESR spectral representation of complex **(15) a** at room temperature and **b** at nitrogen temperature

Table 1 ESR spectra of copper(II) complexes

C. no	Copper(II) complexes	$g_{\parallel}$	$g_{\perp}$	g_{av}	G
7	$C_{32}H_{30}Br_2N_2O_8Cu$	2.19	2.06	2.10	3.25
11	$C_{32}H_{28}Cl_4N_2O_8Cu$	2.21	2.06	2.11	3.59
15	$C_{34}H_{34}N_4O_{14}Cu$	2.23	2.07	2.12	3.36
19	$C_{40}H_{36}N_2O_8Cu$	2.20	2.06	2.10	3.42

of the complex by having unpaired electron in the d_{x2}-d_{y2} orbital. The g tensor values predicted the ionic ($g_{\parallel} > 2.3$) and covalent ($g_{\parallel} < 2.3$) nature of the complexes. Therefore, the covalent character of the complex **(15)** was supported by the $g_{\parallel}$ value which is less than 2.3. The lesser value of orbital coupling constant in comparison of free copper metal ion (832 cm^{-1}) supported the covalent nature of M-L bonds; it was determined with the help of g_{av} value (2.12) which calculated by the given equation-

$$g_{av} = 1/3(g_{\parallel} + 2g_{\perp})$$

The *G* (anisotropic geometric parameter) value was observed by the given formula which indicates some exchange interactions in copper(II) complexes.

$$G = (g_{\parallel} - 2.0023)/(g_{\perp} - 2.0023)$$

Hathway and Billing says that there is negligible interaction in copper metal ions if $G > 4$ and significant exchange interaction between Cu(II) centres if the value of $G < 4$ in the solid state. Here, the value of G was 3.36 which give an idea about exchange interaction in copper(II) metal complex.

Biological investigations

In the present time, we are continuously facing the onslaught of many microorganisms causing illness which is very serious matter for the scientific community, therefore, to find a significant agent for these diseases, we inspected the synthesized compounds for antioxidant, antimicrobial and anti-inflammatory activities.

Antioxidant activity

The extremely reactive oxygen species (ROS) like peroxide, superoxide and hydroxyl radical were arise in human body because of various biochemical process that damage DNA, proteins, lipids, nucleic acid and another biological molecule which is major cause of numerous serious diseases like diabetes, cancer, Parkinson, Alzheimer, aging, coronary heart disease etc. Therefore, it is important to avert our body from free radical scavenging by taking the enriched antioxidants drugs which can repair and stop the oxidative contamination. Therefore, the derived compounds were analyzed for in vitro antioxidant efficacy [61] in triplicates at the 200, 100, 50, 25, 12.5 µg/mL concentrations by DPPH and ABTS assays taking ascorbic acid as standard drug to find pot a compelling antioxidant

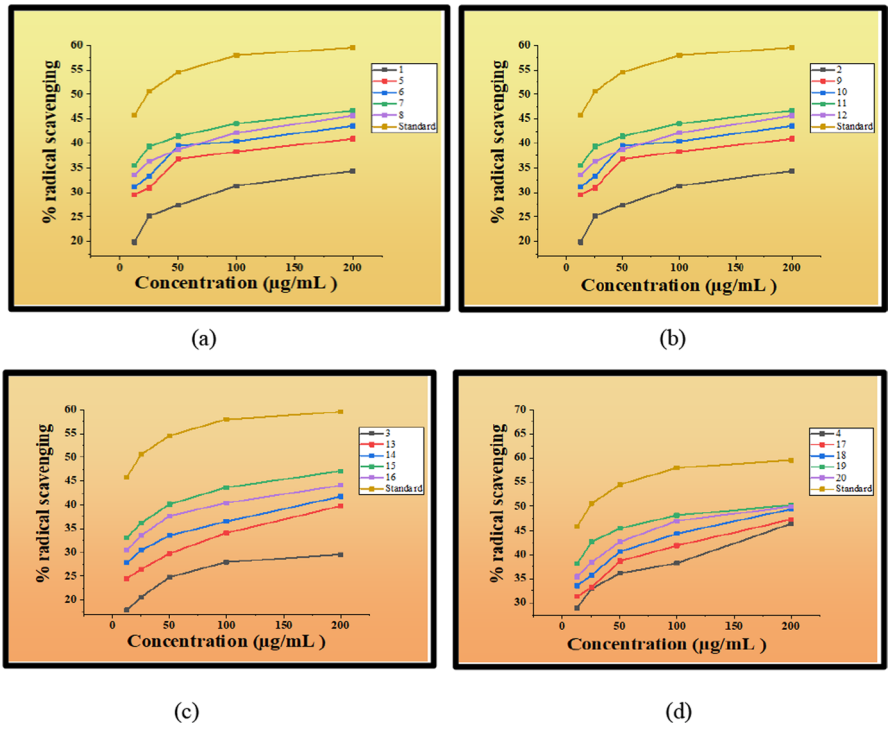

Fig. 5 Graphical representation of concentration (µg/mL) and % radical scavenging data of the compounds **(1–20)** and standard drug

Table 2 Antioxidant values (IC_{50} in μM) of the compounds

C. No	Compounds	IC_{50} (μM ± SD)		C. No	Compounds	IC_{50} (μM ± SD)	
		DPPH assay	ABTS assay			DPPH assay	ABTS assay
1	$C_{16}H_{14}BrNO_3$	8.24 ± 0.03	8.55 ± 0.05	11	$C_{32}H_{28}Cl_4N_2O_8Cu$	6.16 ± 0.02	6.35 ± 0.09
2	$C_{16}H_{13}Cl_2NO_3$	9.33 ± 0.06	9.63 ± 0.07	12	$C_{32}H_{28}Cl_4N_2O_8Zn$	6.56 ± 0.04	6.97 ± 0.05
3	$C_{17}H_{16}N_2O_6$	8.60 ± 0.07	8.96 ± 0.12	13	$C_{34}H_{34}N_4O_{14}Co$	7.99 ± 0.02	8.46 ± 0.02
4	$C_{20}H_{17}NO_3$	7.35 ± 0.01	7.56 ± 0.09	14	$C_{34}H_{34}N_4O_{14}Ni$	7.71 ± 0.08	8.12 ± 0.21
5	$C_{32}H_{30}Br_2N_2O_8Co$	7.47 ± 0.09	7.86 ± 0.05	15	$C_{34}H_{34}N_4O_{14}Cu$	5.80 ± 0.01	5. 76 ± 0.05
6	$C_{32}H_{30}Br_2N_2O_8Ni$	7.09 ± 0.06	7.16 ± 0.08	16	$C_{34}H_{34}N_4O_{14}Zn$	6.71 ± 0.07	6.95 ± 0.06
7	$C_{32}H_{30}Br_2N_2O_8Cu$	6.04 ± 0.10	6.36 ± 0.13	17	$C_{40}H_{36}N_2O_8Co$	5.83 ± 0.10	5.93 ± 0.02
8	$C_{32}H_{30}Br_2N_2O_8Zn$	7.35 ± 0.06	7.33 ± 0.17	18	$C_{40}H_{36}N_2O_8Ni$	5.29 ± 0.04	5.35 ± 0.04
9	$C_{32}H_{28}Cl_4N_2O_8Co$	7.86 ± 0.08	7.75 ± 0.05	19	$C_{40}H_{36}N_2O_8Cu$	4.70 ± 0.07	4.65 ± 0.01
10	$C_{32}H_{28}Cl_4N_2O_8Ni$	6.88 ± 0.02	7.25 ± 0.22	20	$C_{40}H_{36}N_2O_8Zn$	4.94 ± 0.06	5.26 ± 0.05
				21	Ascorbic acid	1.95 ± 0.02	1.98 ± 0.07

agent. The dose dependence data of the compounds were mentioned in Table S5 of the supplementary and the graphical representations was shown in Fig. 5 and the IC_{50} values of the compounds were mentioned in Table 2 and supplementary Fig. S37.

The following conclusions are drawn from the antioxidant activity-

1. The antioxidant evaluation indicates that the activity of all the synthesized compounds and standard drug behave in dose dependence manner which clearly exhibit that the activity of the compounds was enhanced with increasing concentration of the compounds and with decreasing IC_{50} value.
2. The ligands **(1–4)** exhibit the % radical scavenging ability in the region of 17.90 ± 0.11–28.98 ± 0.03 and 29.57 ± 0.09–46.44 ± 0.01 at lower and higher concentrations, respectively and IC_{50} value at 7.35 ± 0.01–9.33 ± 0.06 µM and 7.56 ± 0.09–9.63 ± 0.06 µM in DPPH and ABTS assays, respectively which follows the activity order as $\mathbf{HL^4 > HL^1 > HL^3 > HL^2}$. The most active Schiff base ligand ($\mathbf{HL^4}$) indicate 28.98 ± 0.03 and 46.44 ± 0.01 percentage radical scavenging at lower and higher concentrations, respectively; and IC_{50} value at 7.35 ± 0.01 µM

Table 3 In vitro antimicrobial results (MIC = µmol/mL) of compounds **(1–20) and standard drugs**

C. no	Compounds	Gram (+) bacteria		Gram (−) bacteria		Fungi	
		S. aureus	*B. subtilis*	*E. coli*	*P. aeruginosa*	*R. oryzae*	*C. albicans*
1	$C_{16}H_{14}BrNO_3$	0.0720	0.0720	0.0720	0.0720	0.0360	0.0360
2	$C_{16}H_{13}Cl_2NO_3$	0.0370	0.0370	0.0370	0.0370	0.0185	0.0185
3	$C_{17}H_{16}N_2O_6$	0.0363	0.0363	0.0363	0.0363	0.0181	0.0181
4	$C_{20}H_{17}NO_3$	0.0783	0.0783	0.0783	0.0783	0.0783	0.0783
5	$C_{32}H_{30}Br_2N_2O_8Co$	0.0633	0.0158	0.0633	0.0633	0.0316	0.0316
6	$C_{32}H_{30}Br_2N_2O_8Ni$	0.0634	0.0634	0.0158	0.0634	0.0317	0.0317
7	$C_{32}H_{30}Br_2N_2O_8Cu$	0.0630	0.0630	0.0630	0.0157	0.0315	0.0157
8	$C_{32}H_{30}Br_2N_2O_8Zn$	0.0629	0.0157	0.0629	0.0629	0.0157	0.0078
9	$C_{32}H_{28}Cl_4N_2O_8Co$	0.0162	0.0162	0.0324	0.0162	0.0163	0.0081
10	$C_{32}H_{28}Cl_4N_2O_8Ni$	0.0162	0.0325	0.0325	0.0325	0.0081	0.0162
11	$C_{32}H_{28}Cl_4N_2O_8Cu$	0.0161	0.0323	0.0161	0.0323	0.0080	0.0161
12	$C_{32}H_{28}Cl_4N_2O_8Zn$	0.0080	0.0160	0.0080	0.0160	0.0080	0.0040
13	$C_{34}H_{34}N_4O_{14}Co$	0.0320	0.0320	0.0320	0.0320	0.0320	0.0320
14	$C_{34}H_{34}N_4O_{14}Ni$	0.0320	0.0320	0.0160	0.0320	0.0320	0.0320
15	$C_{34}H_{34}N_4O_{14}Cu$	0.0159	0.0318	0.0318	0.0159	0.0079	0.0079
16	$C_{34}H_{34}N_4O_{14}Zn$	0.0159	0.0318	0.0159	0.0318	0.0318	0.0079
17	$C_{40}H_{36}N_2O_8Co$	0.0683	0.0683	0.0683	0.0683	0.0683	0.0683
18	$C_{40}H_{36}N_2O_8Ni$	0.0684	0.0684	0.0684	0.0684	0.0684	0.0684
19	$C_{40}H_{36}N_2O_8Cu$	0.0679	0.0679	0.0679	0.0679	0.0679	0.0679
20	$C_{40}H_{36}N_2O_8Zn$	0.0678	0.0678	0.0678	0.0678	0.0678	0.0678
21	Ciprofloxacin	0.0047	0.0047	0.0047	0.0047	–	–
22	Fluconazole	–	–	–	–	0.0051	0.0102

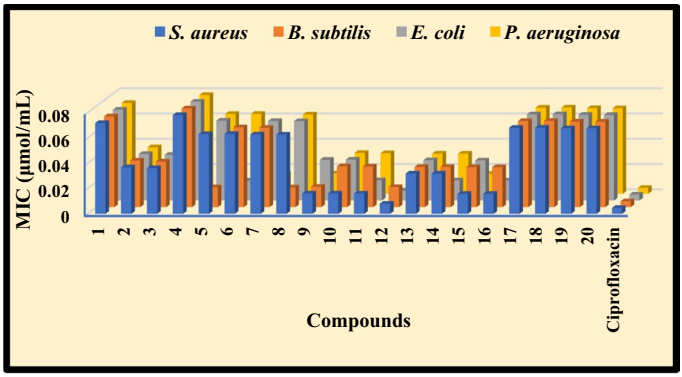

(a)

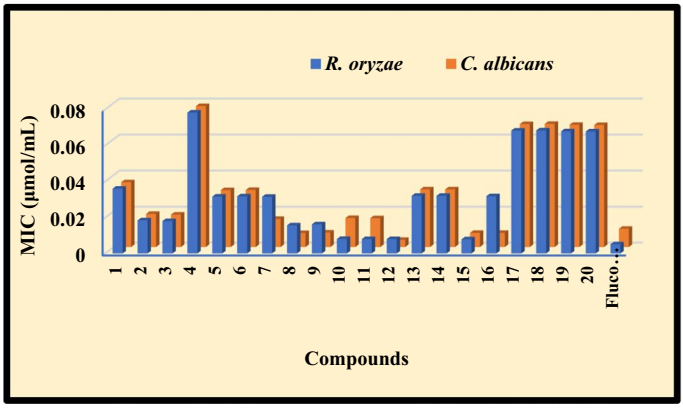

(b)

Fig. 6 **a** Antibacterial **b** antifungal activities of the standard drugs and compounds **(1–20)**

and 7.56 ± 0.09 µM in DPPH and ABTS assays, respectively because of the presence of electron donating groups in the moiety [62].

3. The antioxidant potency of the ligands was increased on complex formation in the region of 24.53 ± 0.08–38.11 ± 0.03 and 39.79 ± 0.06–50.25 ± 0.10 at lower and higher concentrations, respectively with IC_{50} value at 4.70 ± 0.07–7.99 ± 0.02 µM and 4.65 ± 0.01–8.46 ± 0.02 µM in the DPPH and ABTS assays, respectively because of the polarity, metallic effect, hydrophobicity, lipophilicity and spreading of negative charge of –OH group on the aromatic ring.
4. The potency of metal compounds was assessed in the following manner **Cu-(II) > Zn(II) > Ni(II) > Co(II)** due to the ability of the compounds to donate hydrogen atom for disturbance of free radical sequence. The **15, 17, 18, 19, 20** compounds have significant IC_{50} value at 4.70 ± 0.07–5.83 ± 0.10 µM and 4.65 ± 0.01–5.93 ± 0.02 µM in the DPPH and ABTS assays, respectively which are comparable with standard drug.

5. Hence, the result concluded that the synthesized metal complexes have good antioxidant behavior but the copper(II) complex **(19)** (IC_{50} value at 4.70 ± 0.07 µM and 4.65 ± 0.01 µM in the DPPH and ABTS assays, respectively) is highly active species among them which give hopeful therapy for treatment of oxidative stress and pathogenic illness.
6. Further, the comparison of synthesized compounds with previously reported compounds [63–65] revealed that the synthesized compounds (1–20) have more antioxidant activity, so, these may be act as antioxidant agents in health cares.

Antimicrobial activity

The synthesized compounds were examined by serial dilution method using *S. aureus, B. subtilis*, *Escherichia coli, P. aeruginosa*, *R. oryzae, C. albicans* as microbial (bacterial and fungal) strains in triplicates to know their in vitro antimicrobial potency. The fluconazole and ciprofloxacin were utilized as standard drugs for fungi and bacteria, respectively and the obtained results are mentioned as MIC values in Table 3 and Fig. 6.

The results concluded from antimicrobial data are given below-

1. The antimicrobial activity shown by the synthesized compounds is because of the presence of –HC = N- (azomethine) group in the moiety which have a significant role in resamination and transamination of the biological systems. The presence of nitrogen and oxygen donor atoms on the ligands may be prohibit the production of enzyme. According to chelation theory, the polar behavior of the metals decreases because of the partial distribution of its positive charge with ligand upon chelation that increase the lipophilicity of the metal atom and favors their permeability from the lipid layer of cell membrane which enhance antimicrobial potency of the metal complexes [66–68]. Therefore, the chelating behavior of the ligand increase the biological activity on complexation with some another factors like bond length, dipole moment, size of the moiety, hydrophobicity, concentration etc.
2. The synthesized ligands show the antimicrobial results in the following manner $\mathbf{HL^2 > HL^3 > HL^1 > HL^4}$ for all the tested strains of microbes which is due to the electron withdrawing groups attached in the moieties [69, 70].
3. For gram-positive bacteria, the compounds **9, 10, 11, 12, 15, 16** are more potent against *S. aureus* then all the other compounds with MIC value 0.0080–0.0162 µmol/mL and the metal compounds **5, 8, 9, 12** are more potent against *B. subtilis* with MIC value 0.0157–0.162 µmol/mL in comparison of another compounds.
4. For the gram-negative bacteria, the compounds **6, 11, 12, 14, 16** are more active against *E. coli* with MIC value 0.0080–0.0161 µmol/mL and the compounds **7, 9, 12, 15** are more efficient for *P. aeruginosa* with MIC value 0.0157–0.0162 µmol/mL then another compounds.
5. Against fungal strains, **10, 11, 12, 15** complexes are more active for *R. oryzae* with minimum inhibitory concentration value 0.0079–0.0081 µmol/mL and the **8, 9,**

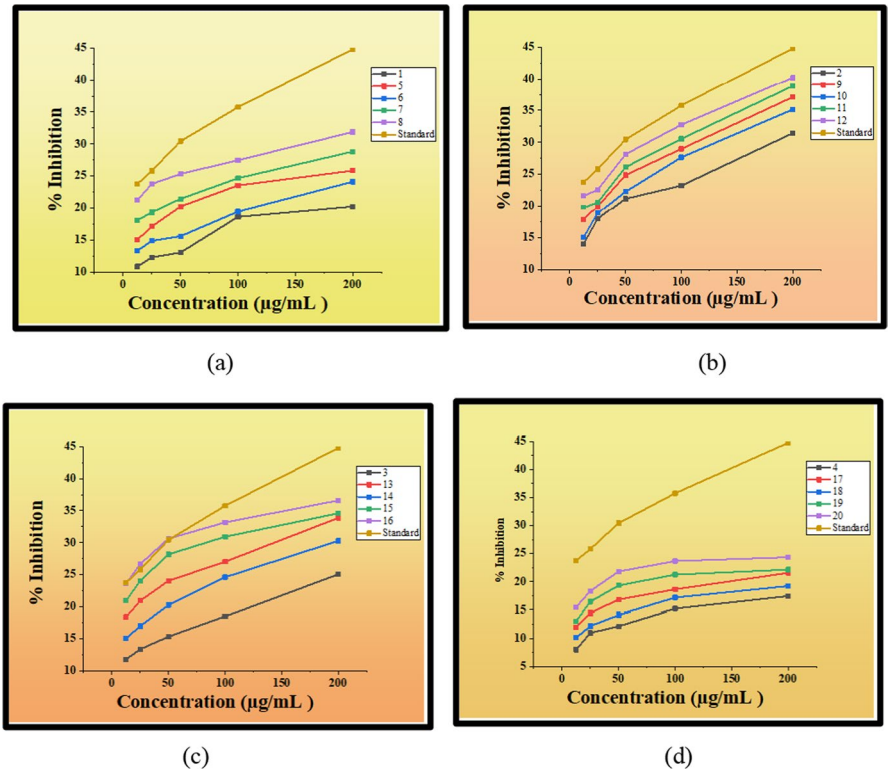

Fig. 7 The percentage inhibition versus concentration (µg/mL) representation of compounds (**1**–**20**) and standard drug

Table 4 Anti-inflammatory activity data (IC_{50} in µM) of ligands, transition metal complexes and standard drug

C. No	Compounds	IC_{50} (µM ± SD)	C. No	Compounds	IC_{50} (µM ± SD)
1	$C_{16}H_{14}BrNO_3$	16.96 ± 0.06	11	$C_{32}H_{28}Cl_4N_2O_8Cu$	7.73 ± 0.04
2	$C_{16}H_{13}Cl_2NO_3$	10.06 ± 0.02	12	$C_{32}H_{28}Cl_4N_2O_8Zn$	7.42 ± 0.02
3	$C_{17}H_{16}N_2O_6$	13.45 ± 0.05	13	$C_{34}H_{34}N_4O_{14}Co$	9.78 ± 0.07
4	$C_{20}H_{17}NO_3$	19.07 ± 0.08	14	$C_{34}H_{34}N_4O_{14}Ni$	10.48 ± 0.08
5	$C_{32}H_{30}Br_2N_2O_8Co$	13.59 ± 0.10	15	$C_{34}H_{34}N_4O_{14}Cu$	9.51 ± 0.04
6	$C_{32}H_{30}Br_2N_2O_8Ni$	15.46 ± 0.07	16	$C_{34}H_{34}N_4O_{14}Zn$	9.11 ± 0.10
7	$C_{32}H_{30}Br_2N_2O_8Cu$	13.28 ± 0.09	17	$C_{40}H_{36}N_2O_8Co$	17.25 ± 0.07
8	$C_{32}H_{30}Br_2N_2O_8Zn$	12.60 ± 0.05	18	$C_{40}H_{36}N_2O_8Ni$	18.28 ± 0.05
9	$C_{32}H_{28}Cl_4N_2O_8Co$	8.10 ± 0.02	19	$C_{40}H_{36}N_2O_8Cu$	16.73 ± 0.01
10	$C_{32}H_{28}Cl_4N_2O_8Ni$	8.34 ± 0.07	20	$C_{40}H_{36}N_2O_8Zn$	15.67 ± 0.03
			21	Diclofenac sodium	6.44 ± 0.02

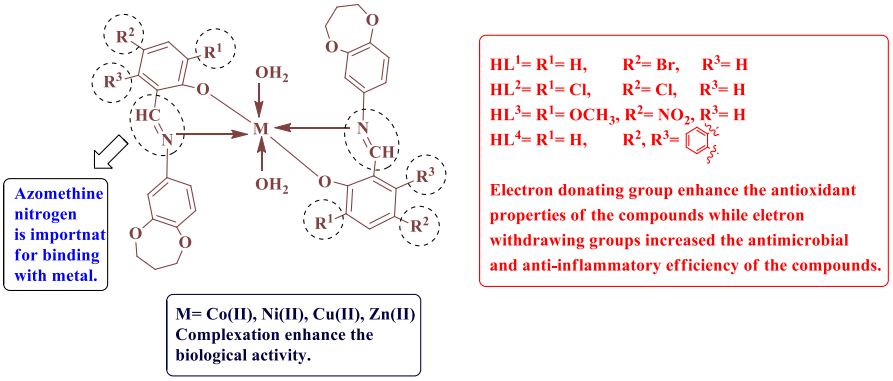

Scheme 2 Structure–activity relationship of the synthesized compounds

12, 15, 16 compounds are active for *C. albicans* with MIC value 0.0040–0.0081 µmol/mL.

6. Among all the synthesized metal compounds, the general trend for reactivity and growth of inhibition against all the tested microbes is **Zn(II) > Cu(II) > Co(II) > Ni(II)** and compound **12** have more activity and least MIC value for all the tested microbes.
7. The more antimicrobial efficacy of the synthesized compounds (1–20) was revealed by comparing the previously reported compounds [71, 72] with synthesized compounds (1–20) which states that the compounds (1–20) have significant MIC values with more antimicrobial activity and may be used to control the microbial dysfunctions in the medicinal industries.

Anti-inflammatory activity

The antimicrobial and anti-inflammatory activities were depended on the electron withdrawing groups of the moieties [73, 74] and the compounds have significant potency against microbial strains, therefore to find out the anti-inflammatory potency of the compounds, the percentage inhibition of the standard drug, ligands and their transition metal compounds were measured on denatured protein by egg albumin assay in triplicates.

Inflammation is the main reason of numerous diseases like cancer, asthma, rheumatoid arthritis etc. which shows the genomic changes and tissue injuries around the infected organs. Therefore, the anti-inflammatory drugs are responsible to destruct the organisms to abolish the irritant from the body and repair the damaged tissues. So, the obtained results are mentioned in Table S6 and Fig. S38 of the supplementary and Fig. 7 and Table 4.

The results revealed the following conclusions-

1. The data of inflammatory evaluation depends on the concentration of the compounds. The percentage inhibition was enhanced with the concentration of the

compounds. The results also shows that the IC_{50} values decreases with increasing percentage inhibition.

2. The ligands (**HL^1**–**HL^4**) indicate the percentage inhibition in the range of 17.44 ± 0.02 to 31.44 ± 0.02% at higher concentration (200 µg/mL) and IC_{50} values from 10.06 ± 0.02 to 19.07 ± 0.08 µM which follows the following activity order **$HL^2 > HL^3 > HL^1 > HL^4$** due to the electron withdrawing groups attached to the moiety.
3. On complexation, the percentage inhibition increased in the range of 19.23 ± 0.12 to 40.21 ± 0.02% at 200 µg/mL concentration which shows IC_{50} values from 7.42 ± 0.02 to 18.28 ± 0.05 µM, suggesting more activity of the compounds in comparison of the ligands for inflammation due to the lipophilicity, metallic effect, ligation behavior, chelation and dispersal of charge.
4. The synthesized complexes show the following order for anti-inflammation **Zn (II) > Cu(II) > Co(II) > Ni(II)** and the **9, 10, 11, 12** compounds have the IC_{50} values very close to standard drug (diclofenac sodium). Compound **12** with IC_{50} value 7.42 ± 0.02 µM is more potent among all the synthesized compounds and might be used for the inflammation ailments.
5. The highest activity of the ligand **HL^2 (2)** and its complexes are explained on the basis of chelation and two electronegative chloro groups of the moiety.
6. Further, we compared the previously reported compounds [75] with the synthesized compounds (1–20) which advocates the more inflammation inhibition ability of the synthesized compounds and revealed that these compounds are many new advancements in the pharmaceutical industry for treating the inflammation causing diseases.

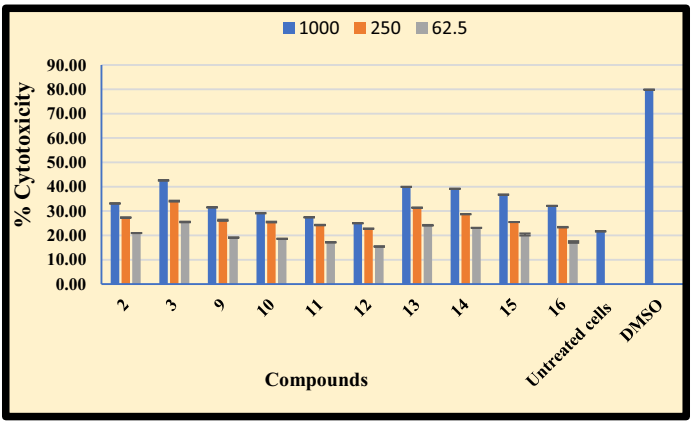

Fig. 8 Cytotoxicity studies of the ligands **(2)**, **(3)** and their metal complexes

Table 5 Cytotoxicity data of highly antimicrobial, anti-inflammatory ligands **(2), (3)** and their **(9–16)** metal complexes

C. No	Compounds	% Cytotoxicity ± SD		
		1000	250	62.5
2	$C_{16}H_{13}Cl_2NO_3$	33.11 ± 0.09	27.33 ± 0.09	20.96 ± 0.05
3	$C_{17}H_{16}N_2O_6$	42.57 ± 0.06	34.08 ± 0.21	25.51 ± 0.16
9	$C_{32}H_{28}Cl_4N_2O_8Co$	31.50 ± 0.01	26.21 ± 0.27	19.10 ± 0.04
10	$C_{32}H_{28}Cl_4N_2O_8Ni$	29.13 ± 0.12	25.48 ± 0.18	18.60 ± 0.11
11	$C_{32}H_{28}Cl_4N_2O_8Cu$	27.42 ± 0.04	24.24 ± 0.13	17.15 ± 0.15
12	$C_{32}H_{28}Cl_4N_2O_8Zn$	24.99 ± 0.03	22.77 ± 0.11	15.43 ± 0.06
13	$C_{34}H_{34}N_4O_{14}Co$	39.95 ± 0.06	31.39 ± 0.11	24.14 ± 0.18
14	$C_{34}H_{34}N_4O_{14}Ni$	39.17 ± 0.03	28.69 ± 0.01	23.11 ± 0.01
15	$C_{34}H_{34}N_4O_{14}Cu$	36.74 ± 0.08	25.48 ± 0.04	20.38 ± 0.45
16	$C_{34}H_{34}N_4O_{14}Zn$	32.15 ± 0.03	23.36 ± 0.14	17.29 ± 0.38

% Cytotoxicity of untreated cells and DMSO are 21.65 ± 0.05 and 79.87 ± 0.08, respectively at 1000 µg/mL concentration

Structure activity relationship

The structure activity relationship was utilized to depict the effect of attached groups on the biological activities of the compounds (Scheme 2). The **(HL^4)** ligand is highly active for antioxidant activity because there is no electron withdrawing group present on the aromatic ring while the presence of bromo group in ligand **(HL^1)** and methoxy, nitro groups in **(HL^3)** ligand justify the moderate efficiencies of the **(HL^1)** and **(HL^3)** ligands, respectively. The lowest antioxidant effect of the **(HL^2)** ligand is justify by the attached electron withdrawing chloro groups at the aromatic ring. Therefore, the antioxidant activity is depends on the electron donating ability of the attached group at the moiety.

The antimicrobial and anti-inflammatory activities are depended on the electron withdrawing group effect of the attached group at the moiety, therefore, the highest antimicrobial and anti-inflammatory potency of the **(HL^2)** ligand is advocated by the presence of two chloro groups at the phenyl ring while the moderate activity are shown by **(HL^3)** and **(HL^1)** ligands as a consequences of methoxy and nitro groups in **(HL^3)** ligand and bromo group in **(HL^1)** ligand. The unsubstituted aromatic ring in **(HL^4)** ligand attributes the least activity of **(HL^4)** ligand.

The performed pharmacological activities show that the biological efficiency of the ligands was enhanced on complexation with transition metal atoms as a consequence of polarity, chelation, hydrophobicity, DNA binding ability, lipophilicity and metallic effect.

Cytotoxicity on Vero cell lines

The in vitro cytotoxicity was performed for highly potent antimicrobial and anti-inflammatory heterocyclic Schiff base ligands **HL^2 (2)** and **HL^3 (3)** and their

Table 6 Number of interactions and binding energy (Kcal/mol) data of ligand **(2)** and its zinc(II) complex **(12)**

Compounds	HL^2 (2) $C_{16}H_{13}Cl_2NO_3$			$[Zn(L^2)_2(H_2O)_2]$ (12) $C_{32}H_{28}Cl_4N_2O_8Zn$		
Target enzymes	*S. aureus* S1: DHFR	*E. coli* DNA gyrase B	*C. albicans* sterol-14-alpha-demethylase	*S. aureus* S1: DHFR	*E. coli* DNA gyrase B	*C. albicans* sterol-14-alpha-demethylase
Binding affinity (kcal/mol)	− 8.9	− 7.7	− 8.4	− 10.2	− 10.1	− 12.6
Interaction with amino acid residues	Ile50, Asn18, Leu20, Ile31, Phe92, Gly94, Gln95	Asn46, Ile78, Lys103, Phe104	Tyr64, Tyr505, His377, Leu376, Leu87, Leu88, Pro230, Leu121, Tyr118	Leu20, Ile14, Gln19	Glu58, Ile60, Asp74, Arg76, Thr163, Lys162, Arg136	Cys470, Gly472, Phe475, Leu150, Gly308, Ile304, Gly307, Gly303, Ile131, Leu376, His377, Met508, Phe233, Pro233

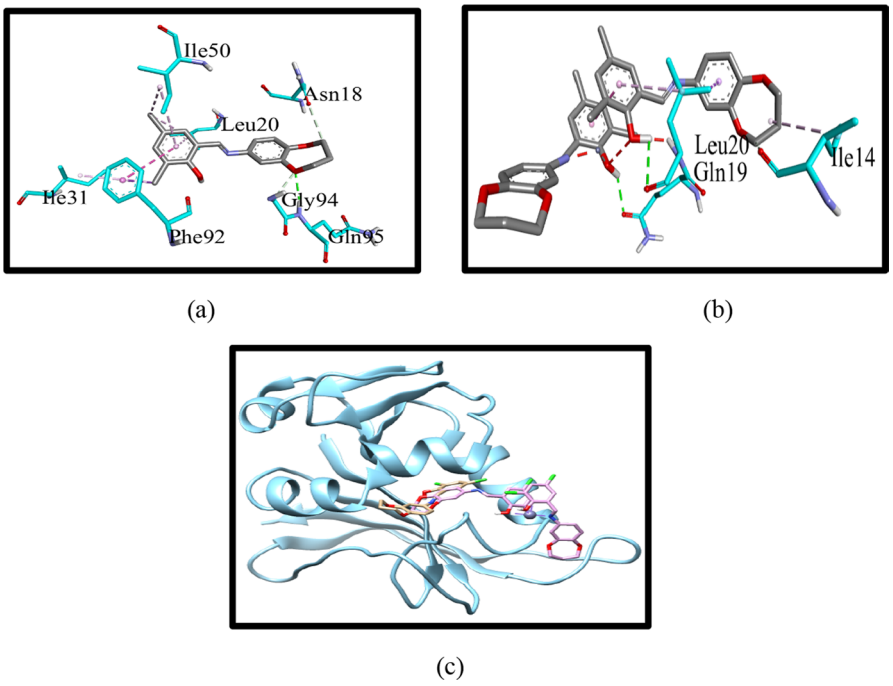

Fig. 9 Binding interactions of **a** ligand **(2)** and **b** complex **(12)** with *S. aureus* S1: DHFR; **c** ligand **(2)** [light brown] and complex **(12)** [pink] representing binding sites with *S. aureus* S1: DHFR [sky blue]

respective transition metal complexes using DMSO as reference on Vero cell lines (Mammalian cells from African Green Monkey Kidney) by calorimetric method in triplicate manner [76]. The cytotoxic data revealed that the toxicity of the compounds behave in the dose dependence manner which decreased with decrease in concentration of the compounds as shown in Fig. 8 and Table 5. The assay shows that metabolic active cells reduced the blue color non-fluorescent resazurin dye into pink color fluorescent resorufin after 4 h of incubation, hence, the optical density measured at 590 nm which was directly depends on the number of viable cells. The obtained data indicates that the Schiff base ligand $\mathbf{HL^2}$ was less toxic than $\mathbf{HL^3}$ at all the treated concentrations due to the different groups present on the phenyl ring, which is also more potent for microbial strains and anti-inflammation. On chelation, the toxicity of the compounds was decreased due to the delocalization of negative charge of –OH group on the phenyl ring, metallic effect and lipophilicity. The cytotoxicity order of the compounds was observed as **Zn(II) < Cu(II) < Ni(II) < Co(II).** The result of the present study indicates that all the compounds are less toxic and have significant properties for medicinal industries, but Zn(II) complex **(12)** is more potent for antimicrobial and anti-inflammatory with very low toxicity at all the treated concentration in comparison of other tested compounds which attracted the attention of the researcher for new drug discovery for some serious diseases.

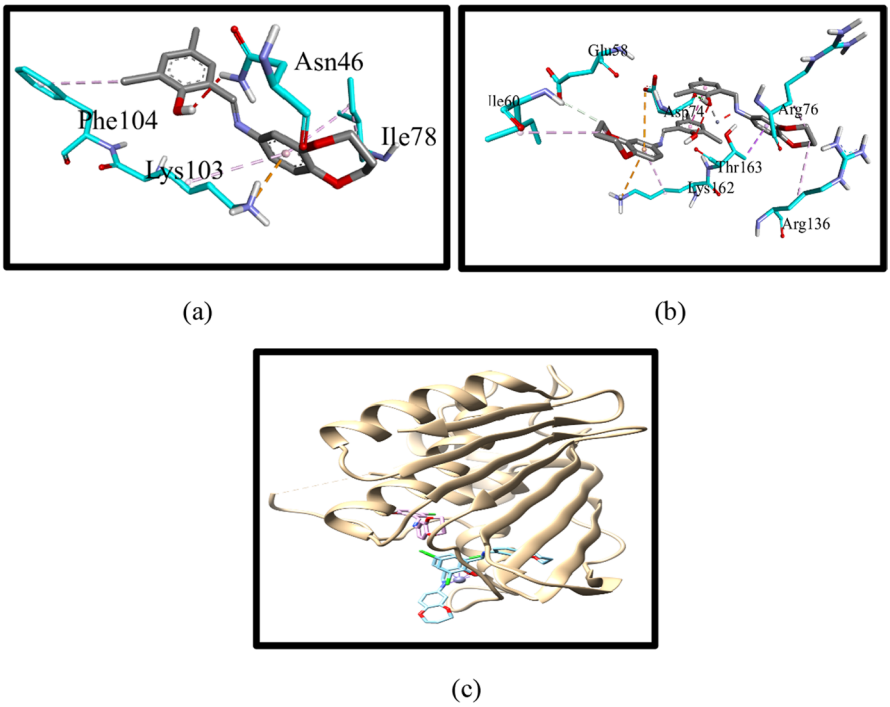

Fig. 10 Binding interactions of **a** ligand **(2)** and **b** complex **(12)** with *E. coli* DNA gyrase B; **c** ligand **(2)** [pink] and complex **(12)** [sky blue] representing binding sites with *E. coli* DNA gyrase B [tan]

Molecular docking

Molecular docking is a computational study and very much demanding in medicinal chemistry. It plays a significant role in drug designing and stimulate the molecular recognition process. Molecular docking is used to evaluate the binding energy that indicates the interaction between the enzyme and ligand molecules. The lower binding energy value indicates the higher binding affinity and more potency of the compounds.

The zinc(II) complex **(12)** $[Zn(L^2)_2(H_2O)_2]$ of heterocyclic Schiff base ligand **(2) (HL^2)** have very low cytotoxicity and more potency for *S. aureus, E. coli* and *C. albicans* strains among tested gram (+) bacteria, gram (-) bacteria and fungus, respectively. Therefore, the evaluation of probable binding score and binding affinity of these compounds is point of interest. To analyze the binding energy of these compounds, three enzymes such as 2W9S, 4DUH, 5TZ1 are chosen for molecular docking studies with respect to *S. aureus, E. coli* and *C. albicans* microbial strains [14, 77, 78]. The molecular docking studies show the various interactions between the compound and amino acid of the enzyme (Table 6 and Figs. 9, 10, 11) which supports the antimicrobial activity and its mechanism of action.

The results of molecular docking are mentioned below-

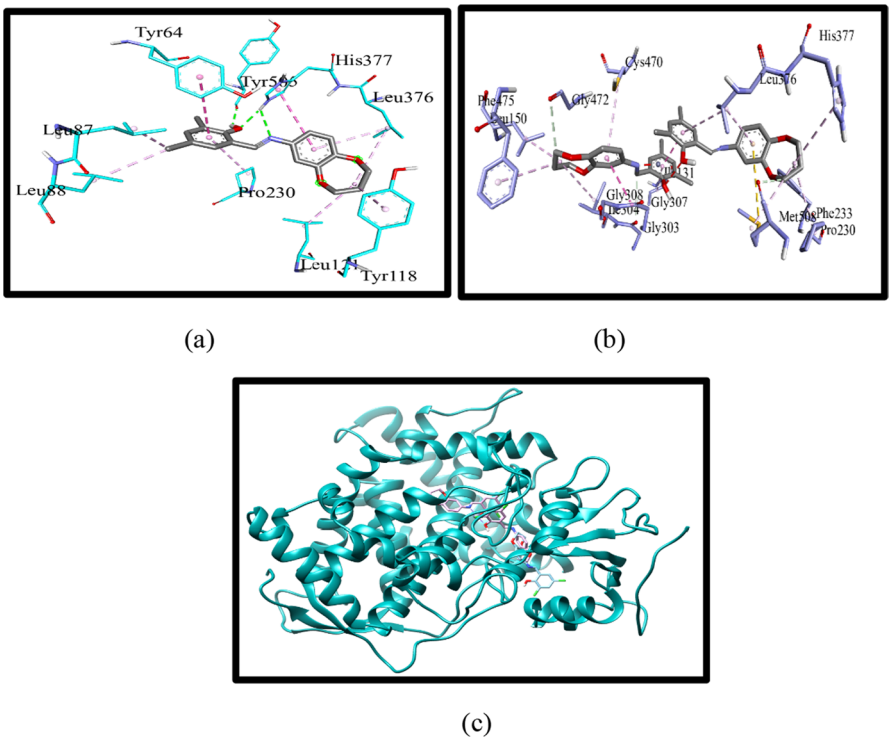

Fig. 11 Binding interactions of **a** ligand **(2)** and **b** complex **(12)** with *C. albicans* sterol-14-alpha-demethylase; **c** ligand **(2)** [light blue] and complex **(12)** [pink] representing binding sites with *C. albicans* sterol-14-alpha-demethylase [cyan blue]

1. For *S. aureus* S1: DHFR, the ligand **(2)** indicates the seven good interaction with the Ile50, Asn18, Leu20, Ile31, Phe92, Gly94, Gln95 residues while on complexation with zinc(II) metal, the complex **(12)** exhibits the Leu20, Ile14, Gln19 interaction. The binding energy of the ligand **(2)** and complex **(12)** was reported at − 8.9 and − 10.2 kcal/mol, respectively.
2. The ligand **(2)** and its complex **(12)** show the binding energy at − 7.7 and − 10.1 kcal/mol, respectively for *E. coli* DNA gyrase B. The ligand **(2)** indicates the four significant interactions with Asn46, Ile78, Lys103, Phe104 amino acid residues and the complex **(12)** have Glu58, Ile60, Asp74, Arg76, Thr163, Lys162, Arg136 interaction with the residues of enzyme.
3. Against *C. albicans* sterol-14-alpha-demethylase enzyme, the ligand **(2)** shows the − 8.4 kcal/mol binding energy and have the nine interactions (Tyr64, Tyr505, His377, Leu376, Leu87, Leu88, Pro230, Leu121, Tyr118) with the active sites of the enzyme. The complex **(12)** indicates the binding energy at − 12.6 kcal/mol and shows the following significant interactions with Cys470, Gly472, Phe475, Leu150, Gly308, Ile304, Gly307, Gly303, Ile131, Leu376, His377, Met508, Phe233, Pro233 residues.

4. From the molecular docking study, we conclude that the binding affinity of the complex is less than the ligand and supports the enhancement of antimicrobial activity on complexation. Among all the three chosen enzymes for docking, complex **(12)** has lowest binding energy (**-12.6** kcal/mol) for *C. albicans* sterol-14-alpha-demethylase enzyme which significantly supports the higher antifungal activity against *C. albicans* and attracted the attention of chemist for synthesis of new antifungal drug.

Conclusion

In the current work, we have synthesized four heterocyclic ligands and their sixteen Co(II), Ni(II), Cu(II) and Zn(II) metal complexes which further characterized by numerous analytical techniques i.e. NMR, FT-IR, mass spectrometry, UV–Vis, TGA, ESR, powder XRD, molar conductivity, elemental analysis and magnetic moment for structure elucidation. The characterization data implies that the complex formation of metal ions occurs with ligands in 1:2 molar ratio forming octahedral geometry which indicates that the ligands coordinated with metal centre in bidentate way from the nitrogen atom of imine linkage and deprotonated phenolic oxygen atom. The biological evaluations strongly advocate that the activity of the ligands was increased on complexation with transition metals. The antioxidant results show that the compounds **15, 17, 18, 19** and **20** are highly antioxidant than the other compounds and the IC_{50} values of these compounds are comparable with standard drug. The antimicrobial evaluation indicates that the compounds **9, 10, 11, 12, 15, 16** are more potent against *S. aureus*; compounds **5, 8, 9, 12** are more active against *B. subtilis*; compounds **6, 11, 12, 14, 16** are highly active against *E. coli*; compounds **7, 9, 12, 15** are more efficient for *P. aeruginosa*; compounds **10, 11, 12, 15** are more active for *R. oryzae*; compounds **8, 9, 12, 15, 16** are highly potent for *C. albicans* then all the other compounds**.** The anti-inflammatory activity revealed that the compounds **9, 10, 11, 12** are more potent and IC_{50} values of these compounds very close to standard drug (diclofenac sodium). Further, in vitro cytotoxicity was analyzed for highly active antimicrobial and anti-inflammatory ligands $\mathbf{HL^2}$ **(2)**, $\mathbf{HL^3}$ **(3)** and their respective metal complexes on Vero cell lines; and found that the complex **(12)** is less cytotoxic than other compounds. The molecular docking study was evaluated for the less toxic and highly antimicrobial active (against *S. aureus* among tested gram (+) bacteria*, E. coli* among tested gram (-) bacteria and *C. albicans* among tested fungal strains) zinc(II) metal complex **(12)** and its ligand **(2)** against the active sites of *S. aureus* S1: DHFR, *E. coli* DNA gyrase B and *C. albicans* sterol-14-alpha-demethylase enzymes which indicate that the compounds have significant binding interactions and validate their biological efficiency. The docking results shows that the ligand **(2)** and complex **(12)** have binding energy at − 8.9 and − 10.2 kcal/mol for *S. aureus* S1: DHFR, − 7.7 and − 10.1 kcal/mol for *E. coli* DNA gyrase B, − 8.4 and − 12.6 kcal/mol for *C. albicans* sterol-14-alpha-demethylase, respectively which are significantly supported the MIC values of antimicrobial activity and confirm that the activity of ligands increases on

complexation. The lowest binding energy of the complex **(12)** against *C. albicans* sterol-14-alpha-demethylase indicate that it is more potent for antifungal activity against *C. albicans* and may be used for fungal deformities in health cares. So, the present research emphasized the biological importance of transition metal complexes of Schiff base ligands in pharmaceutical industries which also advocates by the comparison of previously reported compounds. Hence, this research has an exclusive perception in the constructing of cost-effective, less toxic and more potent medicinal drug for health cares.

Supplementary Information The online version contains supplementary material available at https://doi.org/10.1007/s11164-023-04991-y.

Acknowledgements The author, Mr. Binesh Kumar (File No. 09/752(0105)/2020-EMR-I) is highly thankful to CSIR-HRDG, New Delhi for financial support and also the authors acknowledge to Dr. APJ Abdul Kalam Central Instrumentation Laboratory and Department of Chemistry, Guru Jambheshwar University of Science and Technology, Hisar for providing facilities to carry out this research work.

Authors contributions BK: Data curation, Formal analysis, Investigation, Methodology, Writing-original draft, Software. JD: Supervision, Validation, Writing—review & editing, Data curation. AM: Formal analysis, Investigation.

Funding The author, Mr. Binesh Kumar (File no. 09/752(0105)/2020-EMR-I) is highly thankful to CSIR-HRDG, New Delhi for financial support in the form of senior research fellowship.

Availability of data and materials All the spectra are provided in the supplementary information.

Declarations

Competing interests The authors declare no competing interests.

Ethical approval No animal/human studies were carried out in the present work.

References

1. M. Seki, Org. Process. Res. Dev. **20**, 867 (2016)
2. T. Jurca, E. Marian, L.G. Vicaş, M.E. Mureşan, L. Fritea, Spectrosc. Anal. Dev. Appl. 123 (2017)
3. A. Erxlebe, Inorganica Chim. Acta. **472**, 40 (2018)
4. W.H. Mahmoud, R.G. Deghadi, G.G. Mohamed, Appl. Organomet. Chem. **30**, 221 (2016)
5. I.P. Ejidike, P.A. Ajibade, Rev. Inorg. Chem. **35**, 191 (2015)
6. G. Kumar, S. Devi, D. Kumar, J. Mol. Struct. **1108**, 680 (2016)
7. O. Danilescu, I. Bulhac, S. Shova, G. Novitchi, P. Bourosh, Russ. J. Coord. Chem. **46**, 838 (2020)
8. W.H. Mahmoud, G.G. Mohamed, O.Y. El-Sayed, Appl. Organomet. Chem. **32**, e4051 (2018)
9. M. Lazou, A. Tarushi, P. Gritzapis, G. Psomas, J. Inorg. Biochem. **206**, 111019 (2020)
10. D. Kumar, N. Sharma, M. Nair, J. Biol. Inorg. Chem. **22**, 535 (2017)
11. B. Čobeljić, M. Milenković, A. Pevec, I. Turel, M. Vujčić, B. Janović, K. Anđelković, J. Biol. Inorg. Chem. **21**, 145 (2016)
12. J. Devi, B. Kumar, B. Taxak, Inorg. Chem. Commun. 109208 (2022)
13. A.N. Srivastva, N.P. Singh, C.K. Shriwastaw, Arab. J. Chem. **9**, 48 (2016)
14. J. Devi, S. Kumar, B. Kumar, S. Asija, A. Kumar, Res. Chem. Intermed. **48**, 1541 (2022)
15. S. Bu, G. Jiang, G. Jiang, J. Liu, X. Lin, X. Shen, X. Liao, J. Biol. Inorg. Chem. **25**, 747 (2020)
16. R. Fekri, M. Salehi, A. Asadi, M. Kubicki, Inorganica Chim. Acta. **484**, 245 (2019)
17. Z. Meng, H. Yu, L. Li, W. Tao, H. Chen, M. Wan, P. Yang, D.J. Edmonds, J. Zhong, A. Li, Nat. Commun. **6**, 1 (2015)

18. F.E. Held, A.A. Guryev, T. Fröhlich, F. Hampel, A. Kahnt, C. Hutterer, M. Steingruber, H. Bahsi, C.V. Bojnici-Kninski, D.S. Mattes, T.C. Foertsch, A. Nesterov-Mueller, M. Marschall, S.B. Tsogoeva, Nat. commun. **8**, 1 (2017)
19. E.M. Carvalho, T. de Freitas Paulo, A.S. Saquet, B.L. Abbadi, F.S. Macchi, C.V. Bizarro, V. Bernardes-Génisson, J. Biol. Inorg. Chem. **25**, 887 (2020)
20. U.H. Ramadhan, H.M. Haddad, Z.G. Ezaria, World J. Pharm. Pharm. Sci. **5**, 98 (2006)
21. M. Nath, P.K. Saini, A. Kumar, J. Organomet. Chem. **695**, 1353 (2010)
22. F. Nareetsile, J.T. Matshwele, S. Ndlovu, M. Ngaski, Chem. Rev. lett. **3**, 140 (2020)
23. D.M. Yufanyi, H.S. Abbo, S.J. Titinchi, T. Neville, Coord. Chem. Rev. **414**, 213285 (2020)
24. S. Savir, Z.J. Wei, J.W.K. Liew, I. Vythilingam, Y.A.L. Lim, H.M. Saad, S.S. Kae, K.W. Tan, J. Mol. Struct. **1211**, 128090 (2020)
25. J.M. Méndez-Arriaga, G.M. Esteban-Parra, M.J. Juárez, A. Rodríguez-Diéguez, M. Sánchez-Moreno, J. Isac-García, J. Inorg. Biochem. **175**, 217 (2017)
26. A.A. Garcia-Valdivia, A. García-García, F. Jannus, A. Zabala-Lekuona, J.M. Mendez-Arriaga, B. Fernández, A. Rodriguez-Dieguez, J. Inorg. Biochem. **208**, 111098 (2020)
27. J. Devi, S. Pachwania, J. Yadav, A. Kumar, Phosphorus Sulfur Silicon Relat. Elem. **196**, 119 (2020)
28. L. Deswal, V. Verma, D. Kumar, Y. Deswal, A. Kumar, R. Kumar, M. Bhatia, Chem. Pap. **76**, 7607 (2022)
29. I. Potočňák, P. Vranec, V. Farkasová, D. Sabolová, M. Vataščinová, J. Kudláčová, S.R. Trifunović, J. Inorg. Biochem. **154**, 67 (2016)
30. A. Mumtaz, T. Mahmud, M. Khalid, H. Khan, A. Sadia, M.M. Samra, M.A.R Basra, J. Pharm. Innov. **1** (2020)
31. S. Chandra, P. Chatterjee, P. Dey, S. Bhattacharya, Asian Pac. J. Trop. Biomed. **2**, 178 (2012)
32. P. Kaur, R. Thakur, M. Barnela, M. Chopra, A. Manuja, A. Chaudhury, Chem. Technol. Biotechnol. **90**, 867 (2015)
33. A. Manuja, B. Kumar, T. Riyesh, T.R. Talluri, B.N. Tripathi, Int. J. Biol. Macromol. **165**, 71 (2020)
34. E.F. Pettersen, T.D. Goddard, C.C. Huang, E.C. Meng, G.S. Couch, T.I. Croll, T.E. Ferrin UCSF ChimeraX: Protein Sci. **30**, 70 (2021)
35. I.K. Kareem, M.A. Hadi, Egypt J. Chem. **63**, 301 (2020)
36. M. Munjal, J. Pharmacogn. Phytochem. **7**, 864 (2018)
37. C.T. Prabhakara, S.A. Patil, S.S. Toragalmath, S.M. Kinnal, P.S. Badami, J. Photochem. Photobiol. B Biol. **157**, 1 (2016)
38. J. Devi, S. Sharma, S. Kumar, B. Kumar, D. Kumar, D.K. Jindal, S. Das, Appl. Organomet. Chem. **36**, e6760 (2022)
39. Z. Zhao, J. Zhang, S. Zhi, W. Song, J. Inorg. Biochem. **196**, 110696 (2019)
40. Y. Deswal, S. Asija, A. Dubey, L. Deswal, D. Kumar, D.K. Jindal, J. Devi, J. Mol. Struct. **1253**, 132266 (2022)
41. M. Yadav, S. Sharma, J. Devi, J. Chem. Sci. **133**, 1 (2021)
42. S.E. Abd El-Razek, S.M. El-Gamasy, M. Hassan, M.S. Abdel-Aziz, S.M. Nasr, J. Mol. Struct. **1203**, 127381 (2020)
43. H. Kargar, F. Aghaei-Meybodi, R. Behjatmanesh-Ardakani, M.R. Elahifard, V. Torabi, M. Fallah-Mehrjardi, K.S. Munawar, J. Mol. Struct. **1230**, 129908 (2021)
44. J. Devi, M. Yadav, D. Kumar, L.S. Naik, D.K. Jindal, Appl. Organomet. Chem. **33**, e4693 (2019)
45. K. Singh, M.S. Barwa, P. Tyagi, Eur. J. Med. Chem. **41**, 147 (2006)
46. V.P. Radha, S. Chitra, S. Jonekirubavathi, I.M. Chung, S.H. Kim, M. Prabakaran, J. Coord. Chem. **73**, 1009 (2020)
47. S.G. Nozha, S.M. Morgan, S.A. Ahmed, M.A. El-Mogazy, M.A. Diab, A.Z. El-Sonbati, M.I. Abou-Dobara, J. Mol. Struct. **1227**, 129525 (2021)
48. D. Aggoun, M. Fernández-García, D. López, B. Bouzerafa, Y. Ouennoughi, F. Setifi, A. Ourari, Polyhedron **187**, 114640 (2020)
49. G. Lupaşcu, E. Pahonțu, S. Shova, Bărbuceanu, Ș.F., Badea, M., Paraschivescu, C.E. Dinu-Pîrvu, Appl. Organomet. Chem. **35**, e6149 (2021)
50. J. Devi, N. Batra, Spectrochim. Acta A Mol. Biomol. Spectrosc. **135**, 710 (2015)
51. I. Gonul, M. Kose, G. Ceyhan, S. Serin, Inorg. Chim. Acta. **453**, 522 (2016)
52. C. Vidya Rani, M.P. Kesavan, S. Haseena, R. Varatharaj, J. Rajesh, G. Rajagopal, Appl. Biochem. Biotechnol. **191**, 1515 (2020)
53. J.R. Anacona, J.L. Rodriguez, J. Camus, Spectrochim. Acta A Mol. Biomol. Spectrosc. **129**, 96 (2014)

54. S. Velumani, X. Mathew, P.J. Sebastian, S.K. Narayandass, D. Mangalaraj, Sol. Energy Mater Sol. Cells. **76**, 347 (2003)
55. N. Kavitha, P.A. Lakshmi, J. Saudi Chem. Soc. **21**, S457 (2017)
56. M.M. Abo-Aly, A.M. Salem, M.A. Sayed, A.A. Aziz, Spectrochim. Acta A Mol. Biomol. Spectrosc. **136**, 993 (2015)
57. M.S. Refat, H.A. Saad, A.A. Gobouri, M. Alsawat, A.M.A. Adam, S.M. El-Megharbel, J. Mol. Liq. **345**, 117140 (2022)
58. A.A.M. Belal, I.M. El-Deen, N.Y. Farid, R. Zakaria, M.S. Refat, Spectrochim. Acta A Mol. Biomol. Spectrosc. **149**, 771 (2015)
59. N.N. Rao, K. Gopichand, R. Nagaraju, A.M. Ganai, P.V. Rao, Chem. Data Collect. **27**, 100368 (2020)
60. A. Palanimurugan, A. Dhanalakshmi, P. Selvapandian, A. Kulandaisamy, Heliyon **5**, e02039 (2019)
61. V.P. Singh, S. Singh, D.P. Singh, K. Tiwari, M. Mishra, J. Mol. Struct. **1058**, 71 (2014)
62. H.M. Vinusha, S.P. Kollur, H.D. Revanasiddappa, R. Ramu, P.S. Shirahatti, M.N. Prasad, M. Begum, Results Chem. **1**, 100012 (2019)
63. Q.M. Hasi, Y. Fan, X.Q. Yao, D.C. Hu, J.C. Liu, Polyhedron **109**, 75–80 (2016)
64. L.H. Abdel-Rahman, M.S.S. Adam, N. Al-Zaqri, M.R. Shehata, H.E.S. Ahmed, S.K. Mohamed, Arab. J. Chem. **15**, 103737 (2022)
65. G. Kalaiarasi, C. Umadevi, A. Shanmugapriya, P. Kalaivani, F. Dallemer, R. Prabhakaran, Inorganica Chim. Acta **453**, 547 (2016)
66. N. Ganji, S. Daravath, A. Rambabu, K. Venkateswarlu, D.S. Shankar, Inorg. Chem. Commun. **121**, 108247 (2020)
67. L. Wang, C. Hu, L. Shao, Int. J. Nanomed. **12**, 1227 (2017)
68. N. Kumar, S. Asija, Y. Deswal, S. Saroya, A. Kumar, J. Devi, Phosphorus Sulfur Silicon Relat. Elem. **1** (2022)
69. H.F. Abd El-Halim, G.G. Mohamed, M.N. Anwar, Appl. Organomet. Chem. **32**, e3899 (2018)
70. Y. Deswal, S. Asija, D. Kumar, D.K. Jindal, G. Chandan, V. Panwar, S. Saroya, N. Kumar, Res. Chem. Intermed. **48**, 703 (2022)
71. S. Slassi, A. El-Ghayoury, M. Aarjane, K. Yamni, A. Amine, Appl. Organomet. Chem. **34**, e5503 (2020)
72. A.N. Kursunlu, E. Guler, F. Sevgi, B. Ozkalp, J. Mol. Struct. **1048**, 476 (2013)
73. S.S. Hassan, P.A. Khalf-Alla, Appl. Organomet. Chem. **34**, e5432 (2020)
74. J. Devi, J. Yadav, N. Singh, Res. Chem. Intermed. **45**, 3943 (2019)
75. M.S. Kasare, P.P. Dhavan, B.L. Jadhav, S.D. Pawar, Synth. Commun. **49**, 3311 (2019)
76. A. Manuja, N. Rathore, S. Choudhary, B. Kumar, Med. Chem. **17**, 576 (2021)
77. P. Jain, S. Sharma, N. Kumar, N. Misra, Appl. Organomet. Chem. **34**, e5736 (2020)
78. M.J. Ahmad, S.F. Hassan, R.U. Nisa, K. Ayub, M.S. Nadeem, S. Nazir, U. Rashid, Med. Chem. Res. **25**, 1877 (2016)

Authors and Affiliations

Binesh Kumar[1] · Jai Devi[1] · Anju Manuja[2]

✉ Jai Devi
jaidevi2005@gjust.org; jaya.gju@gmail.com

Binesh Kumar
bineshchemistry131@gmail.com

Anju Manuja
amanuja@rediffmail.com

[1] Department of Chemistry, Guru Jambheshwar University of Science and Technology, Hisar, Haryana 125001, India

[2] ICAR-National Research Centre On Equines, Hisar, Haryana 125001, India